RSC Applied Polymers

REVIEW

View Article Online
View Journal | View Issue

Cite this: *RSC Appl. Polym.*, 2025, **3**, 1428

Recent advances in polymeric materials with exceptional mechanical performance achieved *via* multiple hydrogen-bonded networks

Pouya Rajaee,[a,b] Ishara Wijesinghe,[a,c] Zhiyong Li[a,b] and Cheng Yan *[a,d]

Received 24th June 2025,
Accepted 28th August 2025

DOI: 10.1039/d5lp00189g

rsc.li/rscapplpolym

The development of light weight polymeric materials with high strength and toughness is a growing research focus. Traditional chemical cross-linking techniques, while improving strength, generally compromise toughness. Particle-based cross-linkers, including small molecules, nanoparticles, or polymer aggregates, on the other hand, can form multiple hydrogen-bonded networks with polymer chains, thereby simultaneously enhancing strength and toughness. In addition to highlighting recent advancements in engineering such networks, this short review addresses the effects of different particle types on the mechanical properties of polymers and highlights key design strategies, performance improvements, and industrial opportunities.

1. Introduction

The development of light weight, strong, tough, and self-healing polymeric materials has drawn increased attention from researchers recently due to their wide applications in manufacture, flexible electronics, transportation, packaging, energy storage and conversion, and biomedical engineering.[1–9] However, achieving a balance between strength and toughness is typically a challenge in polymeric materials, as compared to metallic and ceramic materials.[10,11] This difficulty arises from the classic dilemma of mutually exclusive strength and toughness in most materials.

Introducing dynamic covalent bonds, such as disulphide, oxime ester, imine, borate ester, and others, is an effective way to enable self-healing in molecular structures. Dynamic covalent bonding has been found to significantly speed up healing and increase healing efficiency.[12–15] However, due to the distinct molecular interactions, this process often results in reduced extensibility.[16–19] In contrast, dynamic non-covalent cross-linking, including hydrogen bonds (H-bonds), in polymeric materials can increase strength without compromising toughness and ductility.[20–29] Despite having a lower bond energy than covalent bonds, multiple non-covalent bonds can dramatically alter the structures and properties of polymeric materials.[30] It is primarily through nanoconfinement, a process enabled by multiple non-covalent bonds, that the overall properties of polymeric materials are enhanced.[31]

The dissociation and restoration of H-bonds under mechanical strain distribute the energy of fractures across molecules, leading to self-deformation and exceptional toughness. This finding provides a fundamental design strategy for effectively manufacturing materials with super-high performance using multiple hydrogen bonds.[32,33]

Recent advancements in multiple H-bonds have demonstrated promising ways to enhance mechanical strength, toughness, and healing capabilities without sacrificing material flexibility. In this review, the term "multiple hydrogen-bonded networks" refers to cross-linked polymer systems in which multiple H-bonds are formed with polymer chains by additional particles, such as small molecules, nanoparticles, or polymer aggregates. Such particles act as cross-linkers, providing self-healing, structural stability, and energy dissipation by forming reversible non-covalent bonds between polymer chains. Looking ahead to the future of polymeric materials, this short review explores the most recent advancements in high-performance polymeric materials *via* such networks. Finally, we draw conclusions and present a detailed analysis of the challenges and prospects in the development of hydrogen bond cross-linked polymeric materials.

2. The hydrogen bond and its effect on mechanical behaviour

H-bonds are a common type of intermolecular force in nature and are important to many biological processes, such as protein folding and DNA replication.[34,35] The basic structure

[a]*School of Mechanical, Medical, and Process Engineering, Faculty of Engineering, Queensland University of Technology, 2 George Street, Brisbane, QLD 4000, Australia. E-mail: c2.yan@qut.edu.au, pouya.rajaee@hdr.qut.edu.au, ishara.gedara@hdr.qut.edu.au, zhiyong.li@qut.edu.au*
[b]*Centre for Biomedical Technologies, Queensland University of Technology, 2 George Street, Brisbane, QLD 4000, Australia*
[c]*Faculty of Animal Science and Export Agriculture, Uva Wellassa University of Sri Lanka, Passara Road, Badulla, 90000, Sri Lanka*
[d]*Centre for Materials Science, Queensland University of Technology, 2 George Street, Brisbane, QLD 4000, Australia*

of a hydrogen bond, X–H···Y, comprises a proton donor (X–H, abbreviated as D) and a proton acceptor (Y atom having lone pair electrons, abbreviated as A). Hydrogen bonds are formed when two electronegative atoms are non-covalently attracted to each other. This bonding interaction occurs from the electrostatic attraction between the negatively charged Y atom (δ^-) and the positively charged hydrogen (δ^+ X–H), coupled with the interaction of a lone pair of electrons from the electron-rich Y atom with the σ-antibonding orbital of the X–H bond.[36]

A single hydrogen bond is more powerful than van der Waals forces but not as strong as covalent bonds. The strength of hydrogen bonds can vary significantly depending on factors such as bond angle, distance between atoms, and the electronegativity of the involved atoms, ranging from near-covalent bonds to extremely dynamic interactions.[37–45] In supramolecular bonds, hydrogen bonds have comparatively weak and erratic individual strengths. Consequently, highly dynamic hydrogen bonds are often used to create polymeric materials with good self-healing characteristics but lower strength and stiffness. While H-bonds can produce polymeric materials with performance comparable to covalent polymers, the stability of these bonds requires additional energy to break and reform new hydrogen bonding networks. Thus, while strong hydrogen bonds can produce robust polymeric materials, they may compromise self-healing abilities. To achieve a balance between strength and self-healing capability, multiple hydrogen bonds are of significant interest.[46–48]

3. Polymeric materials with multiple hydrogen-bonded networks

Adding particle-based cross-linkers is a crucial method for producing polymeric materials with hydrogen-bonded networks. Kawakami *et al.*[49] utilized small bispyridine molecules for liquid-crystalline polymers, increasing their mesophase stability. Cross-linkers have since been developed (see Fig. 1). These cross-linkers can improve the properties of polymers through multiple H-bonding.

3.1. The role of small molecules

Small molecules rich in groups containing oxygen, nitrogen or fluorine can be effective cross-linkers in polymers. For example, Liu *et al.*[50] prepared HCPA as a hydrogen-bonded cross-linker for polyvinyl alcohol (PVA), resulting in strong, tough, and self-healable polymeric materials. HCPA, consisting of six amino molecules, formed a strong supramolecular structure within PVA by physically cross-linking PVA chains through multiple hydrogen bonds (Fig. 2a). Increasing HCPA greatly improved the tensile characteristics of PVA: strain at break increased by 173%, toughness by 370%, and tensile strength by 48% at 5 wt% HCPA (Fig. 2b). These findings clearly show that HCPA can simultaneously toughen and strengthen PVA, a process that has been proven to be extremely challenging because of the mutually exclusive mechanisms governing toughness and strength.

The toughening and reinforcing mechanisms of HCPA in PVA were investigated using small-angle X-ray scattering (SAXS) measurements and inspection of the fracture morphologies (Fig. 2c–e). When PVA/HCPA was stretched to 100%, the 2D scattering pattern displayed a size increase and the formation of a wide, loose scattering ring, showing the deformation of HCPA-cross-linked nanodomains. When tensile strain increases, the scattering peak in PVA/HCPA shifted to smaller scatter vectors (q), while PVA showed no significant change. The Guinier radius (R_g) of the H-bonded nanodomains rose steadily, from nearly 22 nm at 0% strain to nearly 30 nm at 100% strain. This characteristic, where energy is efficiently dis-

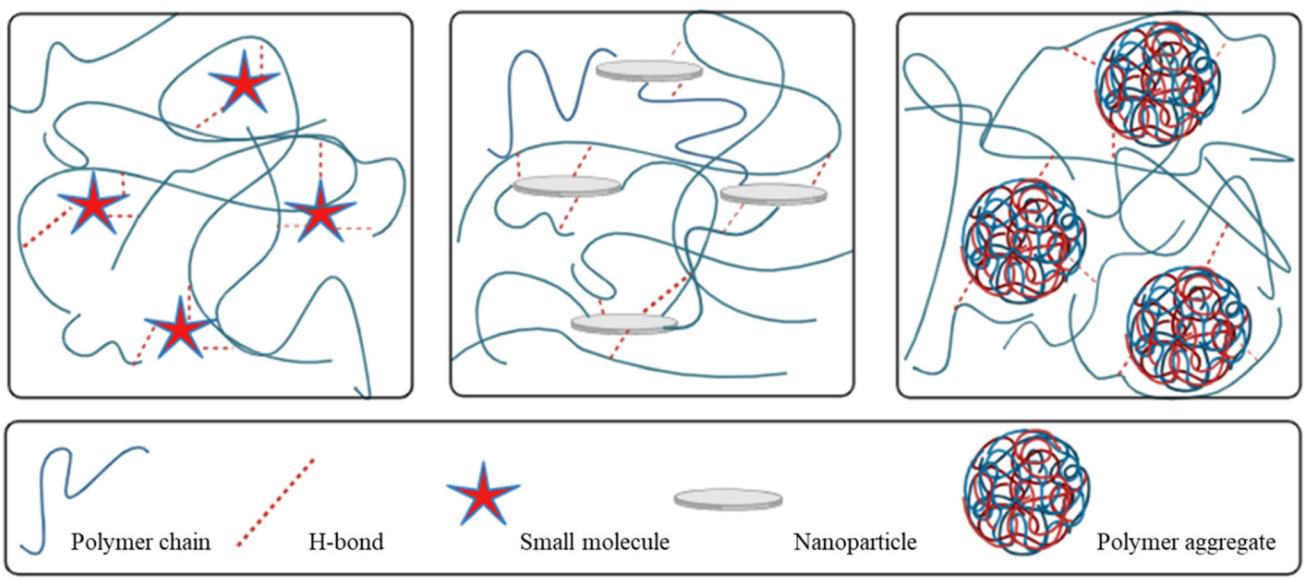

Fig. 1 The H-bond cross-linking of polymeric materials by small molecules, nanoparticles, or polymer aggregates.

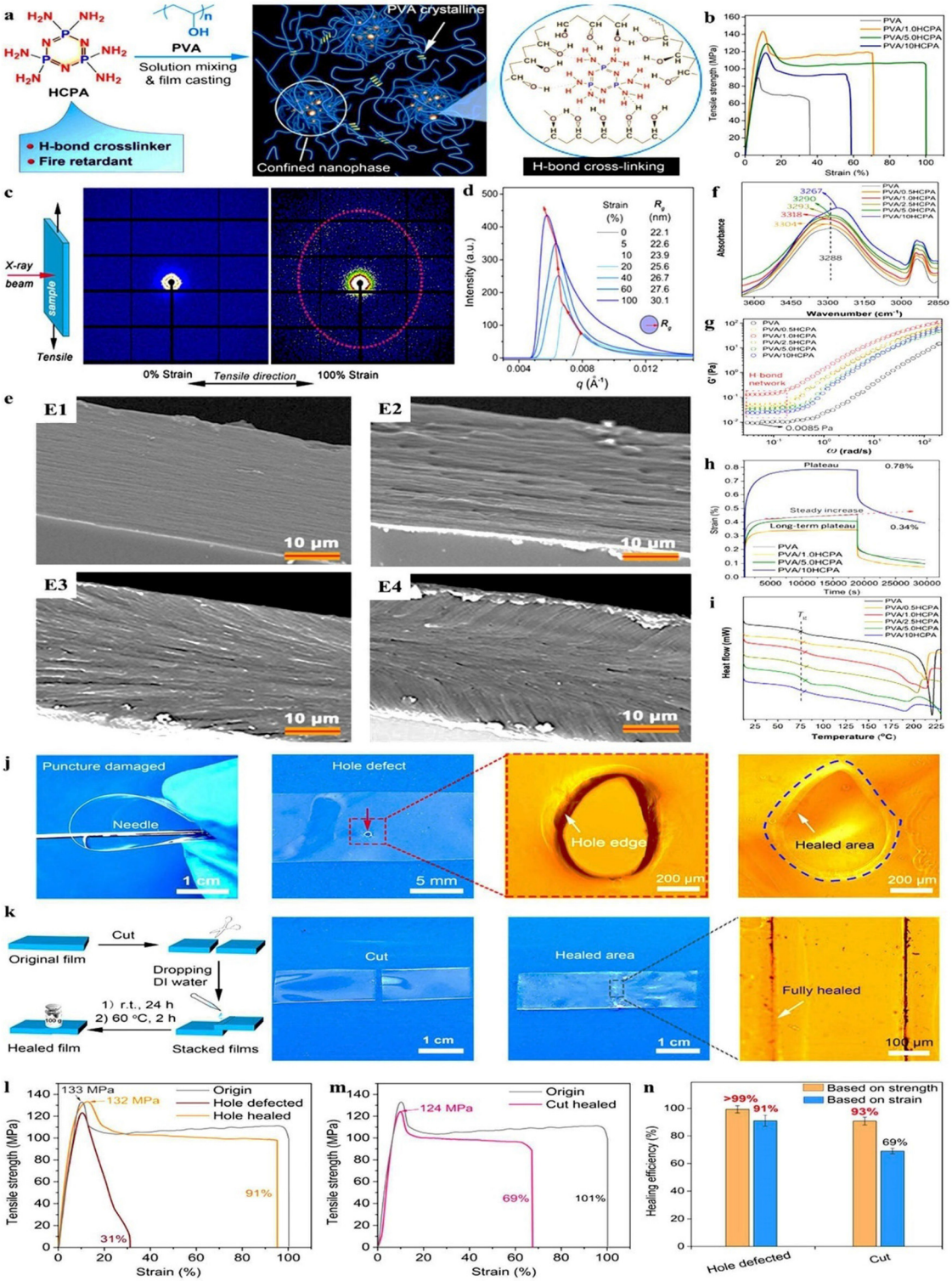

Fig. 2 (a) Diagram showing the synthesis of HCPA as a hydrogen-bonded cross-linker and the process for creating supramolecular PVA/HCPA. (b) Stress–strain curves for PVA/HCPA films. (c) 2D SAXS patterns of PVA with 5 wt% HCPA at 0% and 100% strain. (d) SAXS data illustrating the R_g of nanodomains as a function of tensile strain. (e) Scanning electron microscope (SEM) images of fracture cross-sections of (E1) PVA, (E2) PVA with 1 wt% HCPA, (E3) PVA with 5 wt% HCPA, and (E4) PVA with 10 wt% HCPA after tensile testing. (f) IR spectra for PVA and PVA/HCPA. (g) Frequency dependence of G' on 5 wt% aqueous solutions. (h) Creep and recovery curves for PVA and PVA/HCPA. (i) DSC curves for PVA and PVA/HCPA. (j) Digital and optical photographs of films with puncture damage before and after 24-hour healing at room temperature. (k) Diagram showing cut damage and healing processes, with digital and optical photographs of films before and after 24-hour healing at room temperature and 2 hours at 60 °C. (l and m) Stress–strain curves before and after healing, and (n) healing efficiency. (a–n) Reproduced with permission.[50]

sipated and the formation and propagation of microcracks are inhibited, allows the nanodomains to grow when stretched by breaking and rapidly reconstructing H-bonds between HCPA and PVA.[51] In addition, in contrast to the smooth surface of PVA, the PVA/HCPA fracture morphologies following tensile testing exhibited large-crinkled, network-like structures. This indicates that HCPA-cross-linked nanodomains cause matrix deformation, aiding in the absorption and dissipation of stress energy.

Experimental validation through infrared (IR) spectroscopy, rheological studies, creep and recovery tests, and differential scanning calorimetry (DSC) confirmed the formation of robust hydrogen bonds between HCPA and PVA, as is evident from IR spectroscopy where noticeable blue shifts are observed for the hydroxyl group upon the addition of HCPA[51–55] (Fig. 2f). Rheological investigations revealed a unique 'second plateau' feature of a hydrogen bond-formed cross-linked network[56–59] (Fig. 2g). Lower creep rates were observed in PVA/HCPA during creep and recovery testing, indicating a robust H-bond cross-linked network that reduces deformation over time[60] (Fig. 2h). Thermal analysis showed that the movement of PVA chains was significantly limited by strong H-bonds with HCPA, as indicated by the initial increase in the glass transition temperature (T_g) of PVA with HCPA[61–63] (Fig. 2i). At higher concentrations, there were also slight depressions in T_g, which could isolate PVA chains and weaken interchain interactions, thereby promoting segmental mobility.[56]

Excellent self-healing properties were also observed in PVA/HCPA (Fig. 2j–n). The initial mechanical strength of its films was significantly reduced upon puncture. However, nearly complete recovery occurred when a small amount of H_2O was applied to the damaged region, and the film was left to heal at ambient temperature for 24 h. The healed films greatly outperformed PVA without HCPA, regaining almost 99% of their strength and over 91% of their break strain. Comparable results were also observed following cut damage; after the application of water and subsequent healing, break strain and tensile strength returned by more than 69% and over 93%, respectively, surpassing the recovery rates of PVA.

Liu *et al.*,[64] in another study, developed PVA that combines great toughness, high ductility, and substantial strength using β-cyclodextrin (β-CD) as a hydrogen-bonded cross-linker (Fig. 3a). They investigated how this cross-linker affected the mechanical properties of PVA (Fig. 3b). Initially, PVA exhibited a modulus of about 2 GPa and a strength of 113 MPa. With an increase in β-CD content to 1 wt%, the tensile strength and elastic modulus increase to 136.5 MPa and 3 GPa, respectively. The breaking strain and toughness values reached their maximum at 2 wt% β-CD content, increasing by 397% and 481% over unmodified PVA, respectively. However, higher β-CD levels led to reduced mechanical performance due to β-CD cluster formation decreasing effective hydrogen bonding with PVA. The robust hydrogen bond interactions between β-CD and PVA chains were confirmed by IR spectroscopy, X-ray photoelectron spectroscopy (XPS), DSC, rheological tests, and X-ray diffraction (XRD). For instance, XPS spectra showed that adding β-CD caused the PVA C 1s peak to shift to higher binding energy, indicating hydrogen bond interactions between PVA and β-CD[65,66] (Fig. 3c). The higher C–O content in β-CD resulted in an enhanced ratio of C–C to C–O in PVA with 5 wt% β-CD compared to PVA. XRD analysis using 2 wt% β-CD revealed a decrease in the crystalline size of PVA compounds from 5.33 to 4.25 nm, as hydrogen bond interactions prevented PVA chain rearrangement during crystallization[67] (Fig. 3d). A higher β-CD content marginally increased crystalline size, likely due to PVA bonds being weakened by β-CD aggregation.[68]

Song *et al.*[65] added melamine (MA) to PVA to design polymeric materials with enhanced mechanical properties *via* H-bonded interactions (Fig. 3e). They demonstrated that the yield strength, Young's modulus, strain at failure, and toughness increased significantly with the addition of 1 wt% MA. These values reached approximately 72 MPa, 3 GPa, 110%, and 82 MJ m^{-3}, respectively, which represent increases of 22%, 25%, 144%, and 200% compared to those of PVA (see Fig. 3f). In addition, the study confirmed the H-bonding interactions between the component through IR spectroscopy and rheological studies. Song *et al.*,[56] in another study, demonstrated how four pyrimidine-derived multiamines, including melamine, and small organic cross-linkers could create strong and tough cross-linked PVA (Fig. 3g). The amine groups in each molecule effectively cross-linked PVA through multiple H-bonds. PVA cross-linked with 4N-2456 exhibited significant improvements in yield strength (about 140 MPa), toughness (42 MJ m^{-3}), Young's modulus (3.5 GPa), and strain at break (40%) (Fig. 3h). The results from IR spectroscopy, DSC, and rheological tests confirmed the strong hydrogen bonding interactions between the small organic cross-linkers and PVA chains.

By creating multiple hydrogen bonds between *N*,*N*′,*N*″-tris (2-aminoethyl)phosphoric triamide (TE) and PVA, Xie *et al.*[69] aimed to enhance the mechanical capabilities of PVA and develop a dynamic cross-linking structure in conjunction with the hydroxyl-rich structural characteristics of PVA (Fig. 3i). The PVA/TE compounds were characterized using ^{1}H nuclear magnetic resonance (NMR) and IR spectroscopy to confirm hydrogen bonding interactions. In the ^{1}H NMR spectra of PVA and PVA/TE, the hydroxyl hydrogen resonance peak of PVA appeared as a triplet (chemical shifts at 4.23, 4.46, and 4.68 ppm) (Fig. 3j). These peaks broadened and overlapped to form a single broad peak in the PVA/TE spectrum, indicating hydrogen bonding between PVA and TE. The proton exchange rate slows down during hydrogen bond association, leading to reduced peak intensity and broadening of the resonance peak in the ^{1}H NMR spectra.[71–73] The tensile test results demonstrated that hydrogen bonding improved toughness and strength (Fig. 3k). PVA exhibited a tensile strength of 67 MPa, an elastic modulus of 2.7 GPa, and an elongation at break of 267%. With the creation of a hydrogen-bonded cross-linked network, PVA with 5 wt% TE showed increased strength and modulus (97 MPa and 4.2 GPa), reflecting improvements of 45% and 55%, in turn, and a slight increase in elongation at break to 290%.

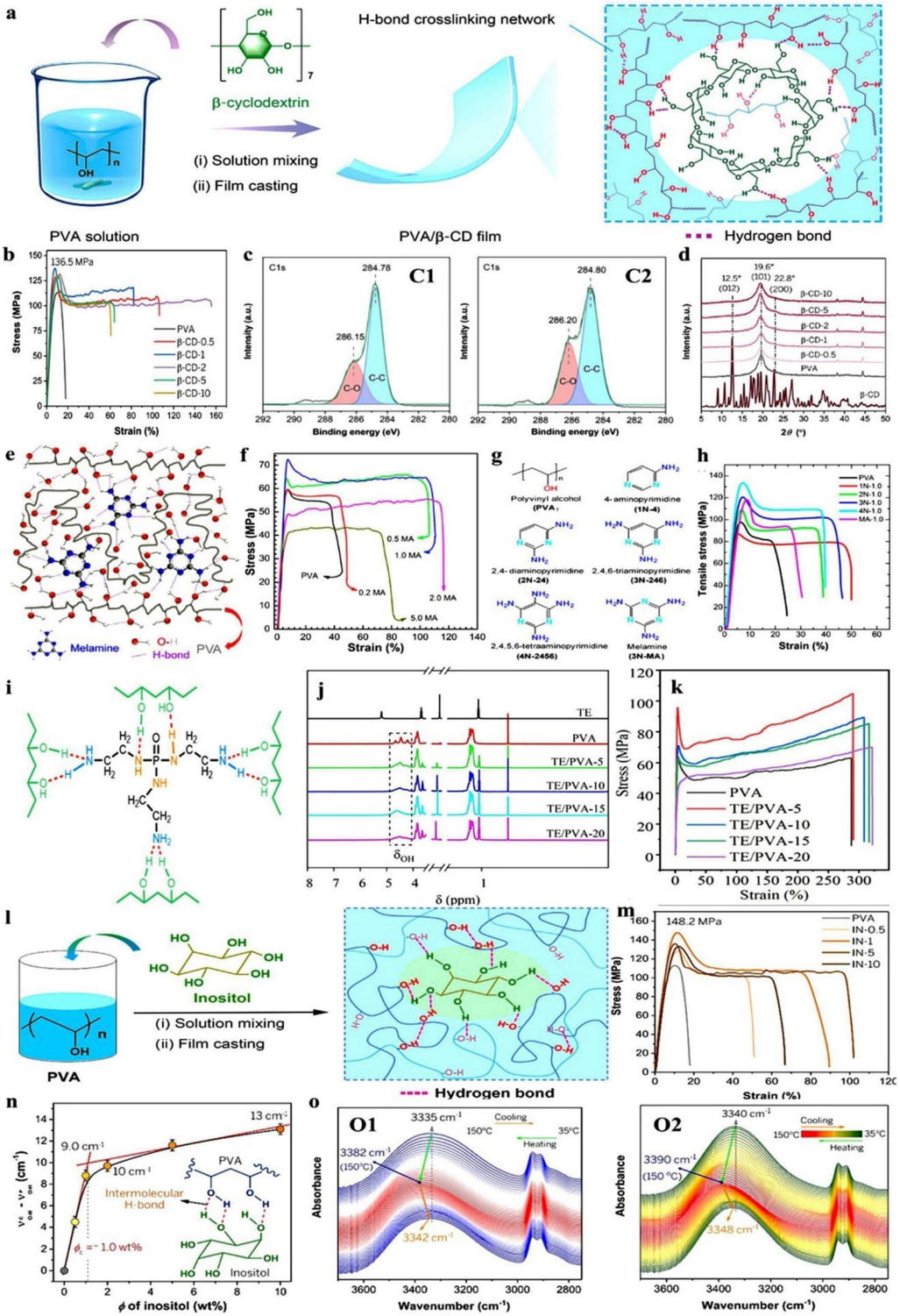

Fig. 3 (a) Diagram illustrating the preparation method for PVA/β-CD films. (b) Stress–strain curves for PVA/β-CD films. (c) High-resolution C 1s elemental scans for (C1) PVA and (C2) PVA with 2 wt% β-CD. (d) XRD patterns for PVA/β-CD films. (a–d) Reproduced with permission.[64] © 2023 Wiley-VCH GmbH. (e) Diagram showing the process for making PVA/melamine (MA) films. (f) Stress–strain curves for PVA/MA films. (e and f) Reproduced with permission.[65] © 2013 American Chemical Society. (g) Structures of PVA and four pyrimidine derivatives, including melamine, used as cross-linkers. (h) Tensile curves for PVA and PVA with 1 wt% of various cross-linkers. (g and h) Reproduced with permission.[56] © 2015 American Chemical Society. (i) Diagram depicting multiple instances of hydrogen bonding between (*N*,*N*′,*N*″-tris(2-aminoethyl)phosphoric triamide (TE)) and PVA. (j) ^{1}H NMR spectra for TE, PVA, and TE/PVA. (k) Stress–strain curves for PVA and TE/PVA. (i–k) Reproduced with permission.[69] © 2021 American Chemical Society. (l) Diagram for the preparation of PVA/inositol (IN) films. (m) Stress–strain curves for PVA/IN films. (n) IR shift observed in PVA/IN films. (o) *In situ* IR spectra for (O1) PVA and (O2) PVA with 1 wt% IN. (l–o) Reproduced with permission.[70] © 2021 American Chemical Society.

Using inositol (IN) molecules as cross-linkers, Xu *et al.*[70] prepared strong and tough PVA (Fig. 3l). The tensile stress–strain curves for PVA/IN are displayed in Fig. 3m. The yield strength initially increased and peaked at 1 wt% IN, reaching 148 MPa, 31% higher than PVA. Although further increases in IN led to a slight reduction in yield strength, it remained higher than that of PVA. The incorporation of IN also caused a brittle-to-ductile transition; the break strain peaked at 86% for 5 wt% IN, compared to 23% for PVA. Consistent with this trend, the elastic modulus peaked at 2.5 GPa at 1 wt% IN. The toughness value reached around 106 MJ m^{-3} for 5 wt% IN, a 5.2-fold increase over PVA. Crucial data about the intermolecular H-bond between PVA and IN were obtained from variable temperature infrared (VTIR) and IR spectroscopy analyses (Fig. 3n and o). The addition of IN to PVA caused a noticeable shift in the ν_{O-H} stretching vibration of the hydroxyl groups in the IR spectra. According to the authors, this shift indicated the replacement of stronger PVA–PVA hydrogen bonds with weaker PVA–IN bonds. VTIR measurements further supported these findings, showing a clear blue shift of ν_{O-H} peaks with increasing temperature. This shift showed the dissociation of some H-bonds and the creation of new, weaker hydrogen bonds or free hydroxyl groups in IN. The shifts, which reverted upon cooling, demonstrated that the H-bonds formed between PVA and IN were thermally stable, even at temperatures as high as 150 °C.[52,74]

By establishing hydrogen bonding with the help of tannic acid (TA), Guo *et al.*[75] successfully fabricated a stretchable, tough, and stiff fluoroelastomer (FE) (Fig. 4a). The mechanical characteristics of the FE were significantly improved by TA (Fig. 4b–e). The elongation at break of the matrix was 634% and increased to a maximum of 1716% at 10 wt% TA, representing a 171% improvement. The toughness of the system also increased, peaking at 34 MJ m^{-3} at 10 wt% TA, approximately three times that of the matrix. Additionally, Young's modulus rose with increasing TA content, reaching a maximum of 6.1 MPa at 15 wt%, more than twice that of the matrix. The study also included a tensile loading–unloading test at 100% strain, which demonstrated the sacrificial nature of the hydrogen bonds (Fig. 4f and g). Each compound exhibited residual strain and notable hysteresis loops in the loading–unloading curves. As the interfacial hydrogen bonds were broken, the hysteresis energy, a measure of energy dissipation, rose with increasing TA content, reaching more than four times the value of the FE at 15 wt% TA. Furthermore, XPS and FTIR spectroscopy were used in this study to confirm the creation of H-bonds in the system.

3.2. The role of nanoparticles

Multiple H-bonding interactions with some polymers can be also facilitated by nanoparticles because of their abundant surface oxygen-containing groups. For example, by uniformly dispersing cellulose nanofiber (CNF) in PVA, Chen *et al.*[76] fabricated a strong and tough nanocomposite based on H-bonding cross-link sites (Fig. 5a). The successful creation of polymeric materials with hydrogen bond cross-linking was confirmed by DSC, IR spectroscopy, and rheological tests. Tensile testing demonstrated that the tensile characteristics of the compounds were greatly improved by the addition of CNF (Fig. 5b and c). PVA showed a tensile stress of 61.8 MPa, a modulus of 3.1 GPa, and a 24.8% elongation at break. These values increased with the addition of 3 wt% CNF, which had an elongation at break of 129.9%, a tensile stress of 160.7 MPa, and a modulus of 5.1 GPa. The authors claimed that these improvements were facilitated by the potent H-bond interaction between PVA and CNF. Moreover, PVA with 3 wt% CNF showed remarkable resistance to breaking under load and toughness. The recyclable and healable characteristics of PVA were also retained in PVA/CNF. PVA with 3 wt% CNF could be dissolved in hot water, filtered, and re-dried for reuse. The nanocomposites only slightly deteriorated after multiple recycling runs, maintaining good mechanical characteristics (Fig. 5d). After seven cycles, there was no discernible loss in ductility and the toughness dropped marginally from 126.3 to 117.2 MJ m^{-3}. The healing properties of recycled PVA/CNF were also analysed by cutting and rejoining the films with water and pressure (Fig. 5e and f). Interestingly, without cracking or deforming, the healed film held a 4.5 kg weight. There was less than a 20% loss in the mechanical parameters of the healed film compared to the original, including strength, strain, modulus, and toughness (Fig. 5g).

Song *et al.*[31] developed graphene oxide dots (GOD) for cross-linking PVA (see Fig. 6a). With an abundance of hydroxyl, epoxide, and carboxyl groups on their surface and edges, GOD can cross-link PVA chains and establish multiple H-bonds with PVA due to the abundance of hydroxyl groups in its macromolecules. Tensile tests were conducted to examine the impact of GOD on the tensile characteristics of PVA films reinforced by GOD (Fig. 6b). Unlike with graphene oxide (GO), the tensile strength and modulus of PVA were improved with GOD without sacrificing ductility. PVA demonstrated a modulus of 2.32 GPa and a yield strength of 91.8 MPa. These values were enhanced to 3.76 GPa and 136.3 MPa, respectively, by adding 0.57 vol% GOD, and to 4.35 GPa and 152.5 MPa, respectively, by adding 1.16 vol% GOD. Rheological testing indicated a reinforcing effect, with G' of PVA rising approximately linearly with increasing GOD (Fig. 6c). At low frequencies, PVA solutions showed a shallow slope, indicating the creation of a physical cross-linked network. The low-frequency area showed a plateau in G' when the content of GOD surpassed 1 wt%, suggesting that GOD can efficiently create GOD-centred nanoconfinements by cross-linking PVA chains through multiple hydrogen bonds.[56,65,77,78] Despite having greater G' values, this phenomenon was not seen in GO-reinforced PVA. The plateau in rheological tests was eliminated by fewer H-bond sites of GO and its steric hindrance, disrupting the hydrogen bonds of PVA.[79] For GOD-reinforced PVA, IR spectra showed notable blue shifts in the hydroxyl stretching vibration, indicating strong H-bond interactions (Fig. 6d). Conversely, GO-reinforced PVA displayed slight changes due to fewer intermolecular connections and weaker H-bond interactions. Due to strong multiple hydrogen bonding interactions, limiting PVA chain mobility, the T_g of

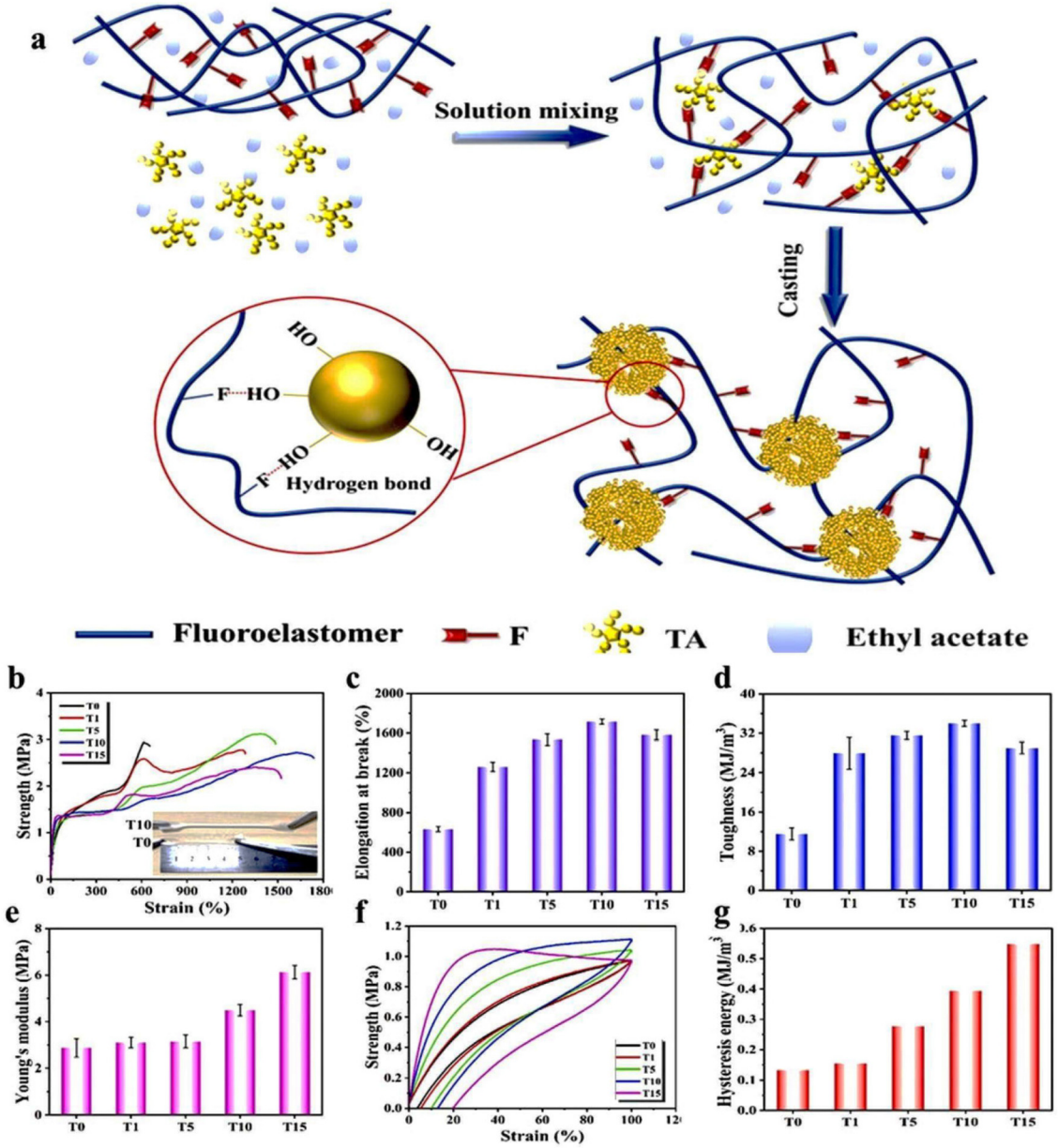

Fig. 4 (a) Schematic diagram illustrating the fabrication process of fluoroelastomer/tannic acid (TA) films. (b) Stress–strain curves (inset shows photographs of fluoroelastomer and fluoroelastomer with 10 wt% TA during stretching), (c) elongation at break, (d) toughness, (e) modulus, (f) loading–unloading curves, and (g) hysteresis energy for fluoroelastomer, fluoroelastomer with 1, 5, 10, and 15 wt% TA. (a–g) Reproduced with permission.[75] © 2023 Elsevier B.V. All rights reserved.

GOD-reinforced PVA also increased with larger GOD content[80,81] (Fig. 6e). In contrast, the addition of GO lowered T_g by weakening and isolating the intermolecular hydrogen bonds among the polymeric chains of PVA.

PVA/aramid nanofibers (ANFs) with high strength and toughness were prepared by Guan *et al.*[82] (Fig. 6f). Increasing ANFs improved the tensile strength and modulus of PVA (Fig. 6g). This enhancement was because of the efficient stress transfer from PVA to ANFs and strong hydrogen bonding interactions that prevent phase separation. However, excessive ANF loading led to decreased tensile strength due to poor dispersion and stress concentration. In addition, PVA/ANFs exhibited higher elongation at break and toughness, attributed to the disruption and reformation of hydrogen bonds and efficient energy dissipation. To investigate PVA and ANF hydrogen bonding characteristics, IR and T_g analyses of PVA nanocomposites were also conducted.

Using maleic anhydride-grafted polypropylene (MA-*g*-PP) and ultrathin two-dimensional (2D) titanium carbide ($Ti_3C_2T_x$) (MXene), Shi *et al.*[83] fabricated nanocomposites with exceptional mechanical properties (Fig. 7a). Results from tensile testing in this study indicated that increased $Ti_3C_2T_x$ loading

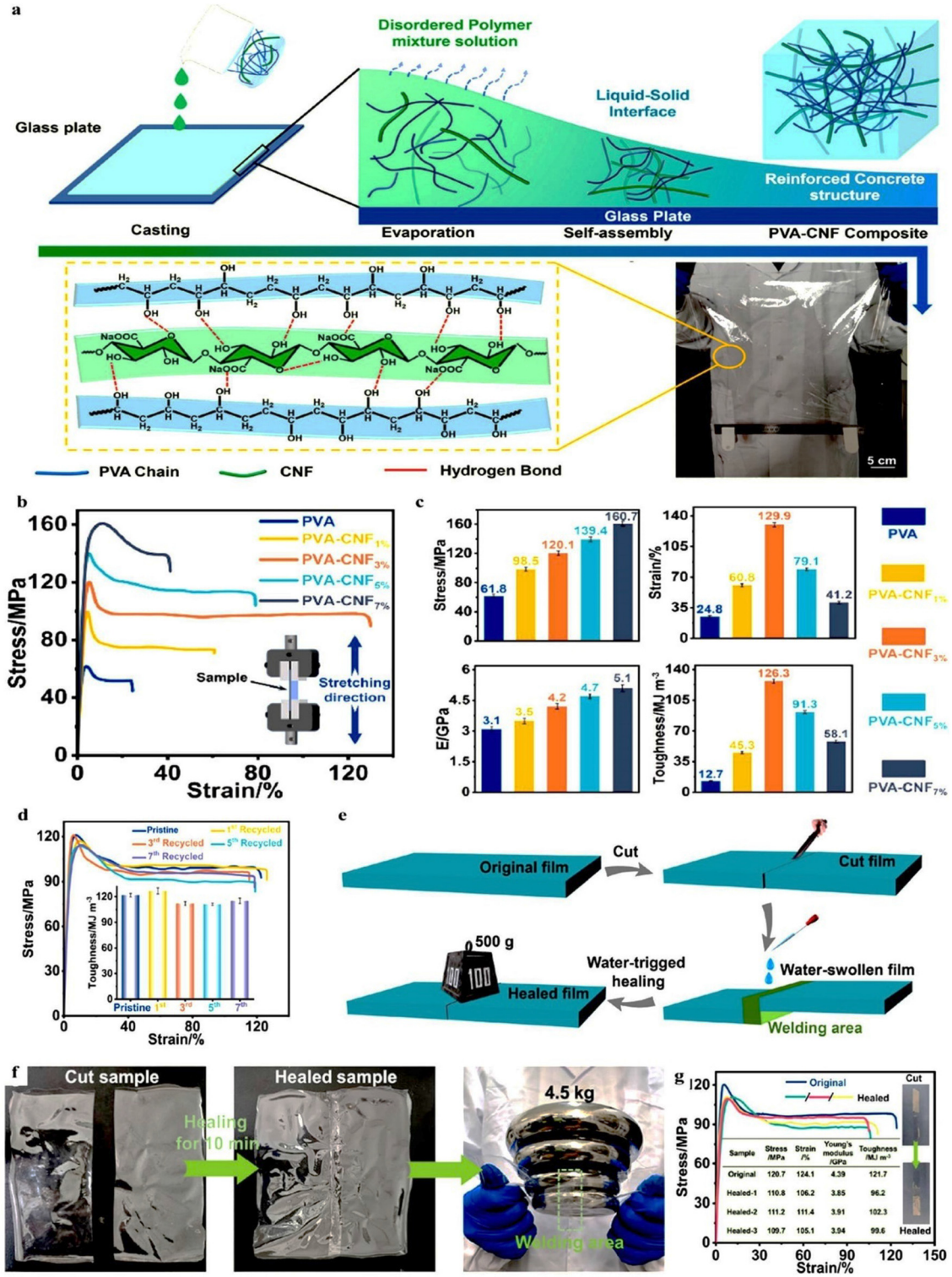

Fig. 5 (a) Preparation process of PVA/CNF nanocomposite film and a digital image of the PVA/CNF nanocomposite. (b) Stress–strain curves of PVA and PVA/CNF nanocomposites. (c) Summary of tensile characteristics of PVA and PVA/CNF nanocomposites. (d) Tensile stress–strain curves of PVA with 3 wt% CNF before and after diverse recycling runs. The inset compares the toughness values of pristine and recycled PVA with 3 wt% CNF. (e) Diagram of the water-assisted healing process for PVA with 3 wt% CNF. (f) Digital images of cut films before and after healing, showing the healed film (60 μm thick) supporting a 4.5 kg weight. (g) Stress–strain curves of original and healed PVA with 3 wt% CNF, with an inset displaying cut and healed strips and a table comparing the tensile characteristics of the original and healed strips. (a–g) Reproduced with permission.[76] © 2023 Elsevier Ltd. All rights reserved.

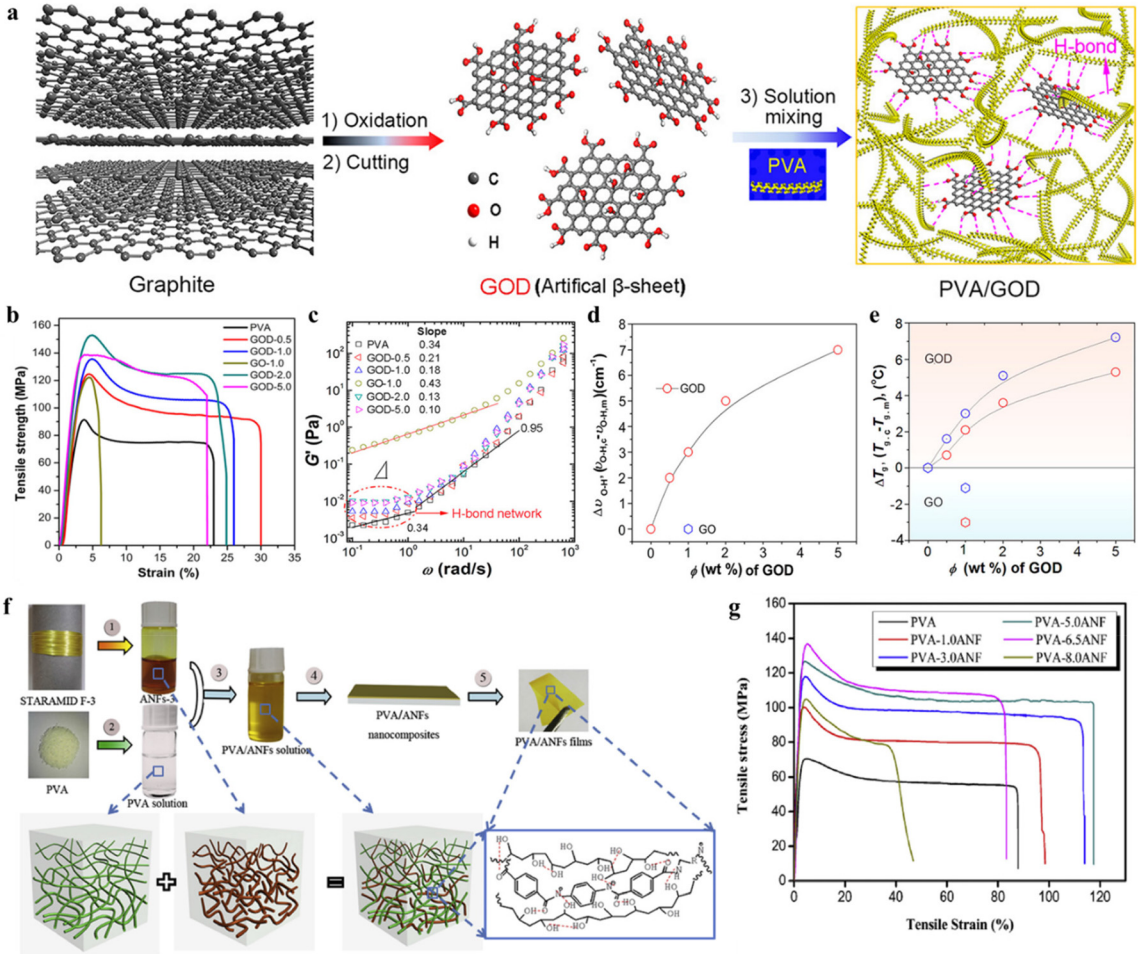

Fig. 6 (a) Diagram showing the synthesis of GOD and the process for fabricating PVA/GOD nanocomposites. (b) Tensile curves of PVA and PVA/GOD. (c) Frequency dependence of G' for PVA and PVA/GOD. (d) Wavenumber shift ($\Delta\nu_{O-H}$) and (e) T_g difference (ΔT_g) of PVA and PVA/GOD compared to PVA. (a–e) Reproduced with permission.[31] © 2018 American Chemical Society. (f) Illustration of interactions between PVA and aramid nanofibers (ANFs). (g) Stress–strain curves of PVA and PVA/ANFs. (f and g) Reproduced with permission.[82] © 2017 Elsevier Ltd. All rights reserved.

generally resulted in an improvement in tensile strength (Fig. 7b). This improvement was documented because of the hydrogen bonding-created structure, limiting the mobility of the polymer chain and improving tensile characteristics. However, elongation at break was marginally reduced in comparison to PP-g, and the ductility trend differed at low $Ti_3C_2T_x$ loading (<1 wt%). On the other hand, elongation at break increased at greater $Ti_3C_2T_x$ levels (>0.5 wt%). According to the authors, it could be inferred from this that increased $Ti_3C_2T_x$ loading provided more slippage sites for nanocomposites to be stretched following tensile testing, breaking hydrogen bonds. To comprehend the load transfer and reinforcing mechanism, this work looked at the fractured surfaces of specimens made of PP-g and its nanocomposite (Fig. 7c). The fractured surface of PP-g was smooth with micro-voids (Fig. 7C1 and C′1), but nanocomposites with low $Ti_3C_2T_x$ exhibited a wrinkled morphology with fewer micro-voids and protruding $Ti_3C_2T_x$ thickly coated with polymeric material, indicating strong interfacial adhesion (Fig. 7C2–4 and C′2–4). An orientated nanosheet structure at 1 wt% $Ti_3C_2T_x$ suggested slippage at the PP-g/$Ti_3C_2T_x$ interface (Fig. 7C′4). In accordance with the findings of tensile tests, an orientated tearing structure was seen at 2 wt% $Ti_3C_2T_x$ (Fig. 7C5 and C′5), indicating the balance between slippage and hydrogen-bonded supramolecular network.

Liu *et al.*[84] functionalized MXene by *in situ* loading nanoscale zirconium amino-tris-(methylenephosphonate) (Zr–AMP) onto its surface for use in polymer nanocomposites based on thermoplastic polyurethane (TPU) (Fig. 8a). They demonstrated that adding functionalized MXene (Zr–MXene) improved the tensile characteristics of TPU (Fig. 8b). The TPU exhibited a tensile toughness of 168 MJ m^{-3}, strain at break of 1500%, and tensile strength of 17.5 MPa. With the addition of 1 wt% Zr–MXene, these values increased to 316 MJ m^{-3} (an 88% boost), 2060% (a 37% rise), and 25.1 MPa (a 43% increase). However, higher Zr–MXene content did not result in further improvements. Cyclical tensile tests were also performed in this study at a fixed strain of 600% to evaluate the anti-fatigue

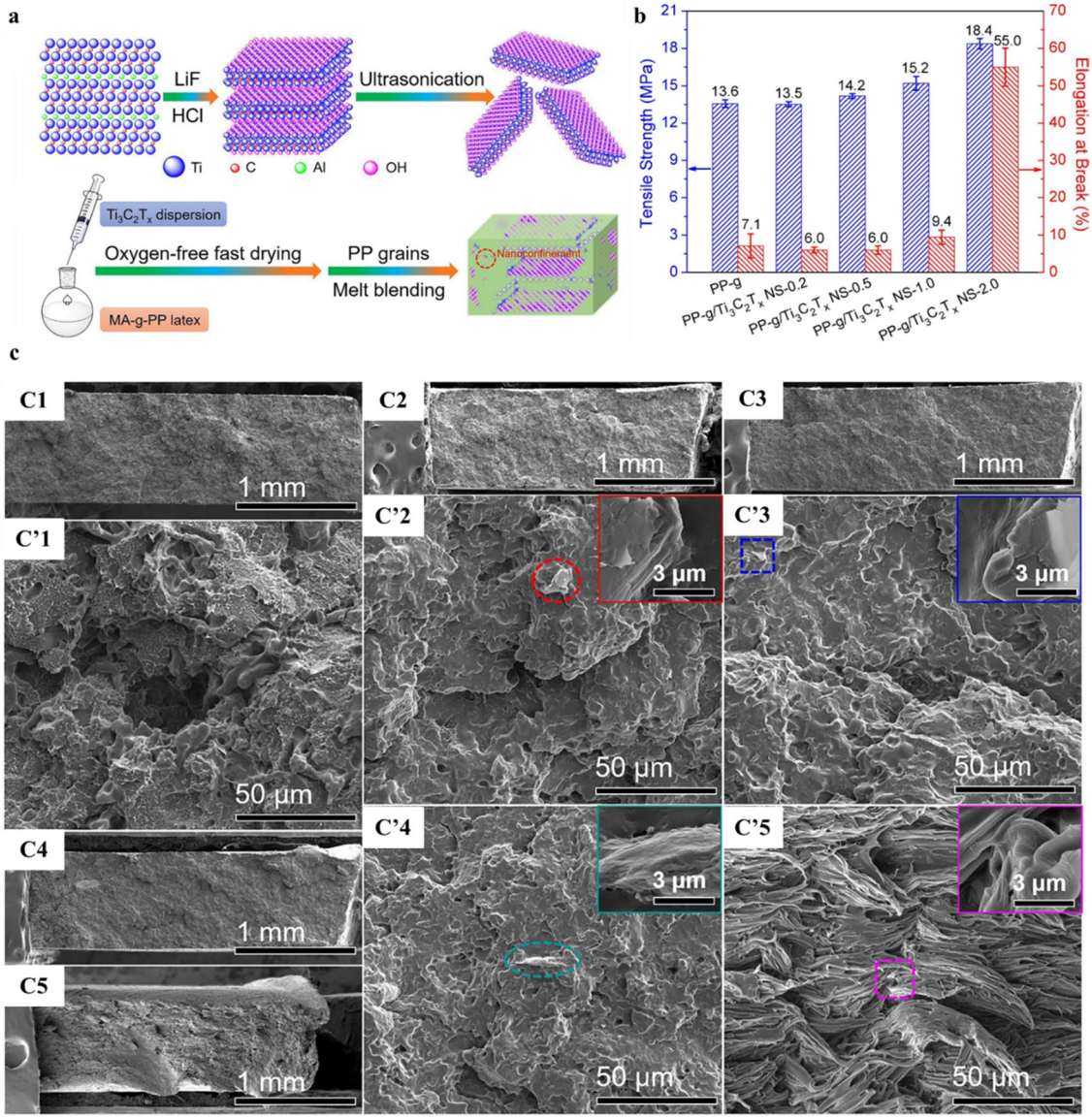

Fig. 7 (a) Diagram showing the synthesis of MXene as a hydrogen-bonded cross-linker and the process for fabricating PP-g/MXene nanocomposites. (b) Tensile properties of PP-g and PP-g/$Ti_3C_2T_x$. (c) SEM photographs of fractured surfaces of (C1 and C′1) PP-g, (C2 and C′2) PP-g with 0.2 wt% $Ti_3C_2T_x$, (C3 and C′3) PP-g with 0.5 wt% $Ti_3C_2T_x$, (C4 and C′4) PP-g with 1 wt% $Ti_3C_2T_x$ and (C5 and C′5) PP-g with 2 wt% $Ti_3C_2T_x$. (a–c) Reproduced with permission.[83] © 2019 Elsevier B.V. All rights reserved.

capabilities of TPU/Zr–MXene (Fig. 8c and d). Tensile strength declined with the number of fatigue cycles due to the incomplete recovery of broken intermolecular connections before the next cycle. After 100 cycles, TPU retained almost 66% of its initial tensile stress; in contrast, TPU/Zr–MXene with 2 wt% Zr–MXene retained roughly 71%, indicating superior fatigue resistance. To further understand how H-bond interactions contribute to the enhanced tensile properties of TPU/Zr–MXene, IR spectra of these materials were recorded.

Liu *et al.*,[85] in another study, produced functionalized $Ti_3C_2T_x$ decorated with 10-(2,5-dihydroxyl phenyl)-9,10-dihydro-9-oxa-10-phosphaphenanthrene-10-oxide (DOPO-HQ) for the fabrication of TPU nanocomposites (see Fig. 8e). They demonstrated how the tensile properties of TPU were affected by the addition of functionalized $Ti_3C_2T_x$ ($Ti_3C_2T_x$–D–H) (Fig. 8f–h). It was found that TPU had a tensile strength of 27 MPa and a break strain of 494%. Due to inadequate interfacial adhesion, adding 4 wt% $Ti_3C_2T_x$ to TPU reduced its tensile strength and break strain. However, these characteristics were enhanced by adding a $Ti_3C_2T_x$–D–H nanohybrid. For example, adding 2 wt% $Ti_3C_2T_x$–D–H improved the tensile strength by 33% to 36 MPa and increased the break strain by 10% to 545.5%. Strong hydrogen bonding with the TPU matrix and good dispersion of the $Ti_3C_2T_x$–D–H nanohybrid were credited for this improvement. Significant improvements were also made to the toughness of nanocomposites; the TPU with

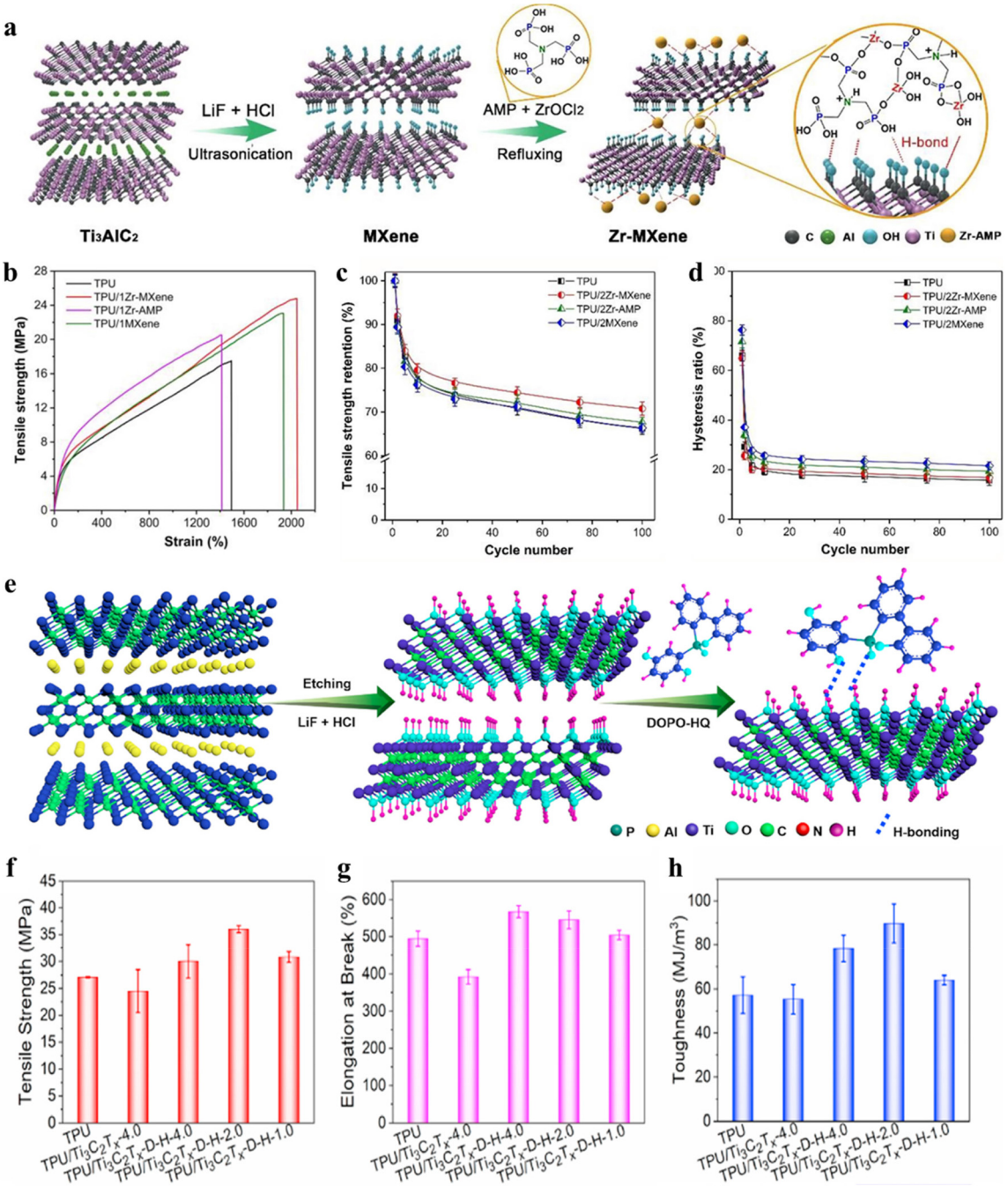

Fig. 8 (a) Diagram showing the synthesis of Zr–MXene; (b) representative stress–strain curves, (c) retention of tensile strength, and (d) hysteresis ratio for TPU, TPU/MXene, and TPU/Zr–MXene. (a–d) Reproduced with permission.[84] © 2021 Elsevier B.V. All rights reserved. (e) Illustration for preparation of $Ti_3C_2T_x$–D–H nanohybrid, (f) tensile strength, (g) elongation at break, and (h) tensile toughness for TPU and TPU/$Ti_3C_2T_x$–D–H. (e–h) Reproduced with permission.[85] © 2022 Elsevier Ltd. All rights reserved.

2 wt% $Ti_3C_2T_x$–D–H showed a toughness of 90 MJ m^{-3}, a 57% increase. To provide evidence of the hydrogen bonding relationship between the $Ti_3C_2T_x$–D–H nanohybrid and TPU, FTIR analysis was performed on the chemical structure of TPU and its nanocomposites.

Epoxidized natural rubber (ENR)/organic-modified layered double hydroxide (O-LDH) polymeric materials with improved mechanical properties were prepared by Li *et al.*[86] (Fig. 9a). The stretching peak of O–H groups and the T_g of the nanocomposites confirmed the formation of a hydrogen-bonded supramolecular network in the ENR/O-LDH. Tensile stress, break strain, and elastic modulus rose to 2.80 MPa, 542%, and 4.70 MPa, respectively, when the O-LDH content in the ENR nanocomposite reached 20 phr (Fig. 9b–d). These values were

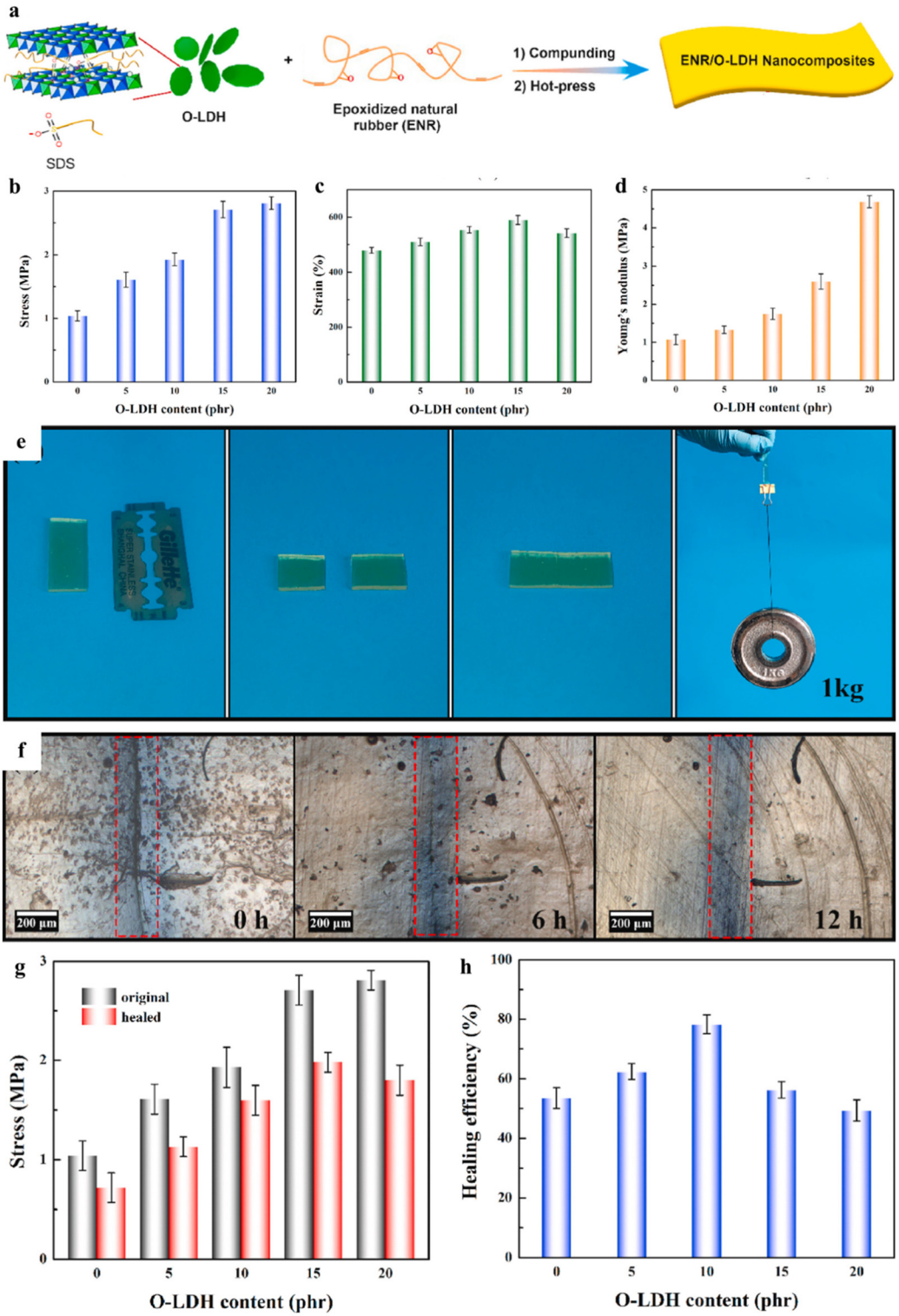

Fig. 9 (a) Illustration of the conceptual design of strong, tough and self-healable ENR/O-LDH nanocomposites; (b) stress, (c) strain, and (d) Young's modulus for ENR/O-LDH. (e) Images of ENR with 10 phr O-LDH following self-healing at 120 °C for 12 hours. (f) Optical microscope images of ENR with 10 phr O-LDH before healing, after 6 hours of healing at 120 °C, and after 12 hours. (g) Stress and (h) healing efficiency for ENR/O-LDH. (a–h) Reproduced with permission.[86] © 2020 Elsevier Ltd. All rights reserved.

366%, 113%, and 427% of those for ENR. The primary cause of this notable improvement in strength and ductility is the reinforcement provided by O-LDH nanosheets and the creation of a dynamic hydrogen-bonded supramolecular network, which allows greater energy dissipation during loading through quick hydrogen bond breakage and recombination.[31,87] Effective self-healing was also demonstrated by ENR/O-LDH (Fig. 9e–h). After 12 hours of healing at 120 °C, the supramolecular network became extremely flexible and was able to support a kilogram of weight. The thermodynamic hydrogen-bonded network and low T_g of ENR, which enable quick chain rearrangement and bond repair, are responsible for the minimal visible damage observed in optical images after healing. Due to limited chain mobility, healing efficiency rose to 10 phr of O-LDH before declining at higher concentrations. The maximum effectiveness of 78% was attained after 12 hours of recovery.

Graphene nanodots (GNDs) were used by Fang *et al.*[88] to manufacture strong and tough poly(ε-caprolactone) (PCL) nanocomposites (Fig. 10a and b). To examine the intermolecular hydrogen bonding interactions between PCL and GNDs, FTIR and XPS tests were performed on the PCL nanocomposites. The tensile stress–strain behaviour of GNDs/PCL revealed that tensile strength and break strain initially increased with GND loading, then marginally decreased (Fig. 10c–e). Tensile strength increased to 27 MPa (a 46% increase over PCL) at 1 wt% GNDs and to 34 MPa (an 82% increase) at 2 wt% GNDs, before slightly decreasing to 23.8 MPa, which was still higher than PCL. The break strain also rose, peaking at 674% at 2 wt% GNDs, which was 46% better than PCL. Similar trends were observed in toughness and elastic modulus, with toughness reaching a maximum of 134 MJ m^{-3} and the elastic modulus reaching a maximum of 380 MPa at 2 wt% GNDs (a 46% increase). SEM examination of fracture morphologies and the enhanced mechanical performance of GNDs/PCL revealed a matrix deformation structure and H-bonded cross-linking network compared to PCL (Fig. 10f–h). A visible 3D H-bonded cross-linking network at the fracture interface and the pull-out of PCL chains were outcomes of the potent nanoconfinement phase around GNDs caused by multiscale H-bond interactions.[89] These multiple H-bond networks caused matrix deformation, crack deflection, and crack tearing, enhancing the strength, ductility, modulus, and toughness of GNDs/PCL.

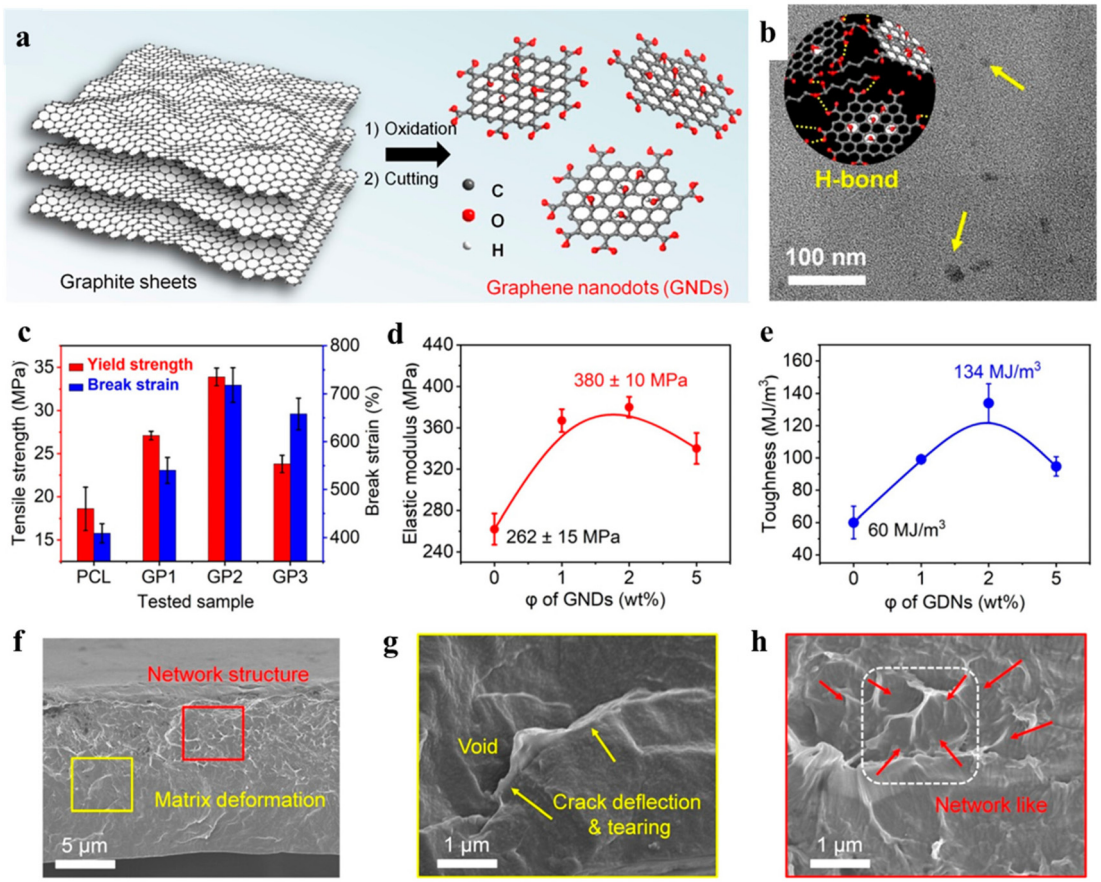

Fig. 10 (a) Diagram showing the synthesis of GOD, (b) the cross-sectional transmission electron microscopy (TEM) image of a PCL/GOD nanocomposite, (c) tensile strength and breaking strain, (d) elastic modulus, and (e) tensile toughness for poly(ε-caprolactone) (PCL) and PCL/graphene nanodots (GNDs). (f–h) SEM photographs displaying the fracture morphology of PCL with 2 wt% GNDs. (a–h) Reproduced with permission.[88] © 2023 American Chemical Society.

3.3. The role of polymer aggregates

Multiple hydrogen-bonded cross-linked polymers can function as efficient cross-linkers for other polymers. For instance, Song *et al.*[90] developed PVA/sulfonated styrene–ethylene/butylene–styrene triblock copolymer (SSEBS) films where sulfonate groups in SSEBS interacted with hydroxyl groups in PVA to form an H-bonded polymer network through multiple hydrogen bonding, as shown in Fig. 11a–d. These interactions were confirmed by rheological data. Tensile strength and breaking strain rose simultaneously when a small quantity of SSEBS was added, as shown in Fig. 11e, due to strong hydrogen bonds and the evenly distributed SSEBS inside PVA (see Fig. 11b–d). When increasing the content of SSEBS to 10 wt%, the H-bonding facilitated improvement in the strain at break of PVA from about 30% to 205% without sacrificing strength, resulting in a toughness of 122 J g^{-1}. However, because of the reinforcing and plasticizing effects of SSEBS, adding more SSEBS rapidly reduced strength and extensibility.

Zhang *et al.*[51] prepared polymeric materials by adding biomass-derived lignosulfonic acid (LA) into PVA (Fig. 11f). The tensile behaviour of PVA/LA was studied, showing significant enhancements in strength, modulus, and toughness compared to PVA (Fig. 11g). The elongation at break was improved from 238% to 361% with only a 1 wt% addition of LA; however, it rapidly decreased with increasing LA. With 5 wt% LA, the tensile strength and modulus were enhanced by 79% and 90% over PVA, in turn, to their highest values of 98.2 MPa and 3.37 GPa. The authors found that the stiff 3D molecular structure of LA and a robust H-bonded network correlated with the greatest mechanical performance in PVA with 5 wt% LA. IR spectra and rheological studies were utilized to determine H-bond interactions between PVA and LA.

Strong and tough PVA containing polydopamine (PDA) were fabricated by Xiong *et al.*[91] (Fig. 11h). Fig. 11i illustrates the

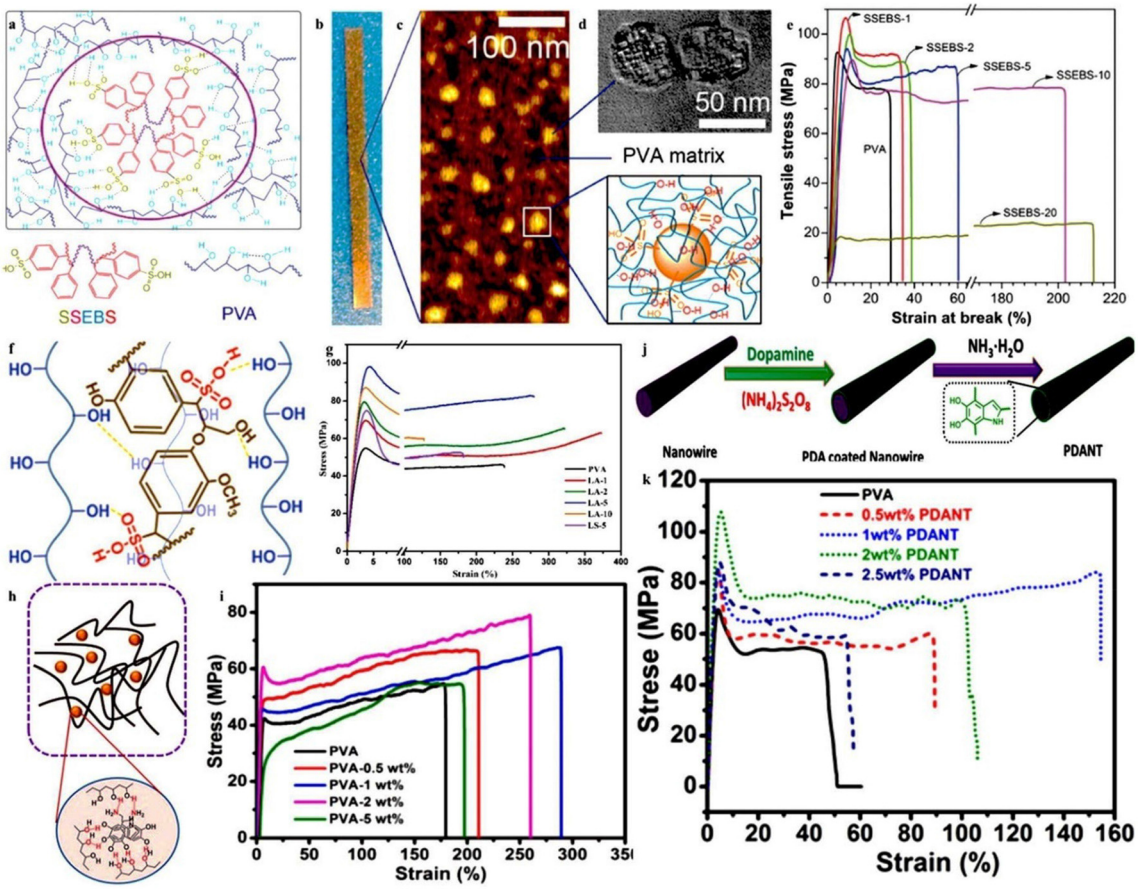

Fig. 11 (a) Diagram showing the formation of multiple hydrogen bonds among PVA and SSEBS. (b–d) Digital and atomic force microscopy (AFM) images of PVA containing 10 wt% evenly distributed SSEBS, along with a TEM image illustrating the self-assembly of SSEBS into phase-separated domains. (e) Stress–strain curves for PVA and PVA/SSEBS. (a–e) Reproduced with permission.[90] © 2017 Wiley-VCH Verlag GmbH & Co. KGaA, Weinheim. (f) Diagram depicting the hydrogen bonds in PVA/biomass-derived lignosulfonic acid (LA). (g) Stress–strain curves for PVA/LA. (f and g) Reproduced with permission.[51] © 2018 Wiley-VCH Verlag GmbH & Co. KGaA, Weinheim. (h) Diagram showing the creation of multiple H-bonds between PVA and polydopamine (PDA). (i) Representative tensile curves for PDA/PVA. (h and i) Reproduced with permission.[91] © 2021 Elsevier Ltd. All rights reserved. (j) Overview of the fabrication process for a polydopamine nanotube (PDANT). (k) Representative stress–strain curves for PVA and PDANT/PVA. (j and k) Reproduced with permission.[92] © 2020 Elsevier Ltd. All rights reserved.

tensile behaviour, such as tensile strength and modulus, elongation at break, and toughness. Stress–strain curves for PVA with less than 2 wt% PDA were comparable to those of PVA, demonstrating a yield at low strain followed by strain hardening. However, the yielding stage vanished at 5 wt% PDA, showing a notable alteration in the PVA characteristics. PVA showed an elongation at break of 168%, a toughness of 83 MJ m^{-3}, a tensile strength of 54 MPa, and a modulus of 1.67 GPa. These characteristics improved with less than 2 wt% PDA; for example, PVA with 2 wt% PDA demonstrated improvements of 43% and 66%, respectively, in tensile strength (77 MPa) and tensile modulus (2.77 GPa). Its elongation at break and toughness were also improved by nearly 55% and 105%, reaching 260% and 170 MJ m^{-3}. However, at 5 wt% PDA, mechanical properties declined due to the increase of amorphous PVA. Evidence for the development of an H-bonding cross-linking network came from IR measurements and rheological experiments.

Fang *et al.*[92] prepared a polydopamine nanotube (PDANT)/PVA composite with improved mechanical properties using a simple solution-casting method. In this work, ammonium molybdate nanowire was utilized as a template to synthesize PDANT inspired by mussels (Fig. 11j). Through tensile testing, the mechanical characteristics of PDANT/PVA were assessed (Fig. 11k). PVA exhibited a modulus of 3 GPa and a strength of 67 MPa. The addition of PDANT resulted in improvements of approximately 63% and 34%, respectively, in strength and modulus up to an ideal content of 2 wt%, where the strength reached 109 MPa and the modulus 4.01 GPa. The authors ascribed this improvement to hydrogen bonds between PDANT and the matrix, enhanced crystallinity, and the higher mechanical qualities of cross-linked polydopamine. The breaking strain and toughness of PDANT/PVA also improved dramatically. For instance, PVA containing 1 wt% PDANT demonstrated a toughness of 110.2 MJ m^{-3} and an ultimate strain of 122%, which were increases of 144% and 324%, respectively, over PVA. IR spectra confirmed the H-bond interactions between PDANT and PVA chains.

4. Comparative analysis of particle-based cross-linkers and multiscale hydrogen-bond synergy

Direct comparison of the tensile properties of reported multiple hydrogen-bonded polymer networks is challenging. This complexity arises from variations in polymer matrices, cross-linker chemistry, filler loadings, processing conditions, mechanical testing protocols, and other factors. To address these inconsistencies, we calculated the percentage improvement in strength, modulus, strain at break, and toughness compared to the neat polymer for each study. This approach gives us a more meaningful evaluation of the trends across various types of cross-linkers. Table 1 displays the values and associated percentage improvements for the studies examined in this work.

Table 1 reveals that small molecules often perform exceptionally well in increasing strain at break and toughness, presumably due to their greater mobility in the polymer matrix, even though they typically provide only moderate reinforcement in strength and modulus. However, in most cases, nanoparticles produce the largest improvements in modulus and strength, attributed to their high aspect ratio, large surface area, and rigid nature. While nanoparticles offer moderate improvements in strain at break and toughness, often lower than those achieved with small molecules, exceptional cases, such as PVA/CNF, exhibit enhanced performance across all properties. Polymer aggregates tend to give balanced improve-

Table 1 Tensile properties and corresponding percentage improvements (Δ) of multiple hydrogen-bonded polymer networks incorporating various particle-based cross-linkers, as reported in the studies reviewed in this work

Cross-linker	Loading	Strength (MPa) (Δ)	Modulus (GPa) (Δ)	Strain at break (%) (Δ)	Toughness (MJ m^{-3}) (Δ)	Ref.
PVA/HCPA	0–10 wt%	90–147 (+63%)	2.1–3.21 (+53%)	36–101 (180%)	24–112 (+367%)	50
PVA/β-CD	0–10 wt%	113–136.5 (+21%)	2–3 (+50%)	22.5–112 (+398%)	20.3–118 (+481%)	64
PVA/MA	0–5 wt%	53.9–65 (+21%)	2.32–2.91 (+25%)	45–109.8 (+144%)	22–66 (+200%)	65
PVA/4N-2456	0–5 wt%	97–138 (+42%)	2.4–3.5 (+46%)	20–40 (+100%)	17–42 (+147%)	56
PVA/TE	0–20 wt%	67–97 (+45%)	2.7–4.2 (+55%)	267–290 (+8%)	NA	69
PVA/IN	0–10 wt%	113–148 (+31%)	2–2.5 (+25%)	23–86 (+274%)	20.3–106 (+422%)	70
FE/TA	0–15 wt%	NA	0.003–0.004 (+50%)	634–1716 (+171%)	11.5–34 (+196%)	75
PVA/CNF	0–7 wt%	61.8–160.7 (+73%)	3.1–5.1 (+64%)	24.8–129.9 (+424%)	12.7–126.3 (+894%)	76
PVA/GOD	0–5 vol%	91.8–152.5 (+66%)	2.32–5.08 (+119%)	23–30 (+30%)	16.8–30.3 (+80%)	31
PVA/ANF	0–8 wt%	70.6–136.6 (+93%)	4.4–5.2 (+18%)	87.9–117.7 (34%)	50.2–124.9 (+148%)	82
PP-g/MXene	0–2 wt%	13.6–18.4 (+35%)	NA	7.1–55 (+675%)	NA	83
ENR/O–LDH	0–20 phr	1.04–2.81 (+170%)	0.001–0.005 (+400%)	480–542 (+13%)	NA	84
TPU/Zr–MXene	0–2 wt%	17.5–25.1 (+43%)	0.011–0.017 (+54%)	1500–2060 (+37%)	168–316 (+88%)	86
TPU/MXene–D–H	0–4 wt%	27.1–36 (+33%)	NA	494.3–545.5 (+10%)	57.2–89.7 (+57%)	87
PCL/GND	0–3 wt%	18.6–33.9 (+82%)	0.262–0.38 (+46%)	461–674 (+46%)	60–134 (+123%)	88
PVA/SSEBS	0–20 wt%	91.2–92.3 (−1%)	1.85–2.41 (−23%)	30–205 (+583%)	17.4–122 (+601%)	90
PVA/LA	0–10 wt%	54.8–98.2 (+79%)	2.3–3.37 (+46%)	238–282 (+18%)	105.9–219.2 (+107%)	51
PVA/PDA	0–5 wt%	54–77 (+43%)	1.67–2.77 (+65%)	168–260 (+56%)	83–170.1 (+105%)	91
PVA/PDANT	0–2.5 wt%	67–109 (+62%)	3–4.01 (+34%)	50–100 (+100%)	26–78 (+200%)	92

ments in strength, modulus, strain at break, and toughness, although some systems, like PVA/SSEBS, differ from this trend.

While the earlier comparison can provide some indication of the individual roles of small molecules, nanoparticles, and polymer-aggregates, their combined effects across different length scales are equally important. Small molecules operate at the molecular scale to make hydrogen bond switching rapid and reversible, thereby improving toughness and ductility.[93] Nanoparticles, which have dimensions in the nano- to submicrometer range, provide high stiffness and strength due to their rigid load-bearing frameworks.[94,95] At the microscale, hydrogen bonding and physical entanglement work together to give polymer aggregates long-term stability and balanced reinforcing.[96] This indicates that using cross-linkers from various scales can lead to synergistic effects. Such multiscale architectures could enable the simultaneous improvement of strength, stiffness, stretchability, and toughness. A notable example is the dynamic nanoconfinement quenching strategy reported by Zhao *et al.*,[97] in which tannic acid, cellulose nanocrystals, and a PVA matrix achieved exceptional improvements over pure PVA in tensile strength (~170%), modulus (~120%), strain at break (~200%), and toughness (~550%). This demonstrates the potential of multiscale synergy to surpass the performance of any single cross-linker type.

5. H-bond metrics and structure–property relationships

As discussed, hydrogen-bonded cross-linked polymers offer a unique ability for mechanical behavior modification. Two significant quantitative metrics that serve as vital links between macroscopic features and molecular-scale interactions are bond strength/energy and bond lifetime/kinetics. The interplay between these two metrics governs the structure–property relationships of H-bonded cross-linked polymers.

By decreasing chain slippage under stress, stronger hydrogen bonds or multiple H-bonds can withstand greater loads before dissociating, improving tensile strength and stiffness.[98] The polymer may behave more like a highly cross-linked network, which can be brittle if there are too many bonds or bonds that are too strong.[99,100] According to one experiment, modulus typically increases as the concentration of H-bonding units in elastomers increases; however, above a critical concentration, extensibility is sacrificed to achieve the increased stiffness.[101] Bonds that are both strong enough to support the network and weak enough to break under load in a controlled way typically exhibit optimal performance.

The lifetime of a hydrogen bond, or how long it typically lasts before dissociating, is another controlling parameter of the time-dependent mechanical properties of H-bonded cross-linked polymers. When these bonds have short lifetimes, they can break and reform quickly, which enhances the material's extensibility and toughness by allowing the chains to shift and absorb energy. On the other hand, longer lifetimes make these H-bonded cross-links function almost like permanent connections in the short term. This stability enables the material to withstand stress better, resulting in increased stiffness and strength, while also slowing down stress relaxation.[102] An ideal balance often arises when the bond lifetime is comparable to the stress relaxation time of the polymer because bonds remain intact under rapid loading but gradually dissociate during slower deformation, maximizing toughness while preventing brittle failure.[103]

In many cases, optimum performance derives from a synergistic combination of these extremes, obtaining the requisite rigidity together with controlled energy dissipation.[104,105] These are the bases for rational polymeric material design specific to the mechanical and functional requirements of specific applications.

6. Applications of polymeric materials with exceptional performance *via* multiple hydrogen-bonded networks

A multitude of technological applications depend on the development of new materials with strong mechanical and self-healing properties. Because of their reversible and dynamic interactions, supramolecular polymers, especially those cross-linked by hydrogen bonds, have become attractive options. These materials exhibit remarkable extensibility, toughness, and strength, making them suitable for a variety of applications.

In the field of biomedicine, for example, hydrogen bonds are essential because they affect the bioactivity and biocompatibility of polymeric materials. Hydrogen bonds promote cell adhesion, proliferation, and differentiation in bone scaffolds by improving the interaction between the scaffold and the surrounding biological environment.[106,107] The biocompatibility of a PVA/HCPE composite was evaluated for its potential use as artificial ligaments by Liu *et al.*[67] Human umbilical vein endothelial cells (HUVECs) cultured on the PVA and PVA/HCPE films for 72 hours showed similar morphologies to the control group, indicating normal cell metabolism (Fig. 12a and b). Fluorescence images confirmed the high viability of HUVECs on the PVA/HCPE films, with cell viability after seven days being greater than that of PVA and similar to that of the control group.

Beyond biomedical uses, multiple hydrogen-bonded networks have been integrated into advanced sensing devices. Utilizing supramolecular multiple H-bonding polymers (MHBP), an extremely responsive and self-repairing sensor for human–machine interaction (HMI) was developed[108] (Fig. 12c). This sensor combined MHBP with a carbon nanotube conducting network in chitosan-decorated epoxy natural rubber latex to establish multiple H-bonds with carboxyl cellulose nanocrystals. The HMI system showed promise for robotic patient support when it was combined with signal-processing software to identify speech and facial expressions.

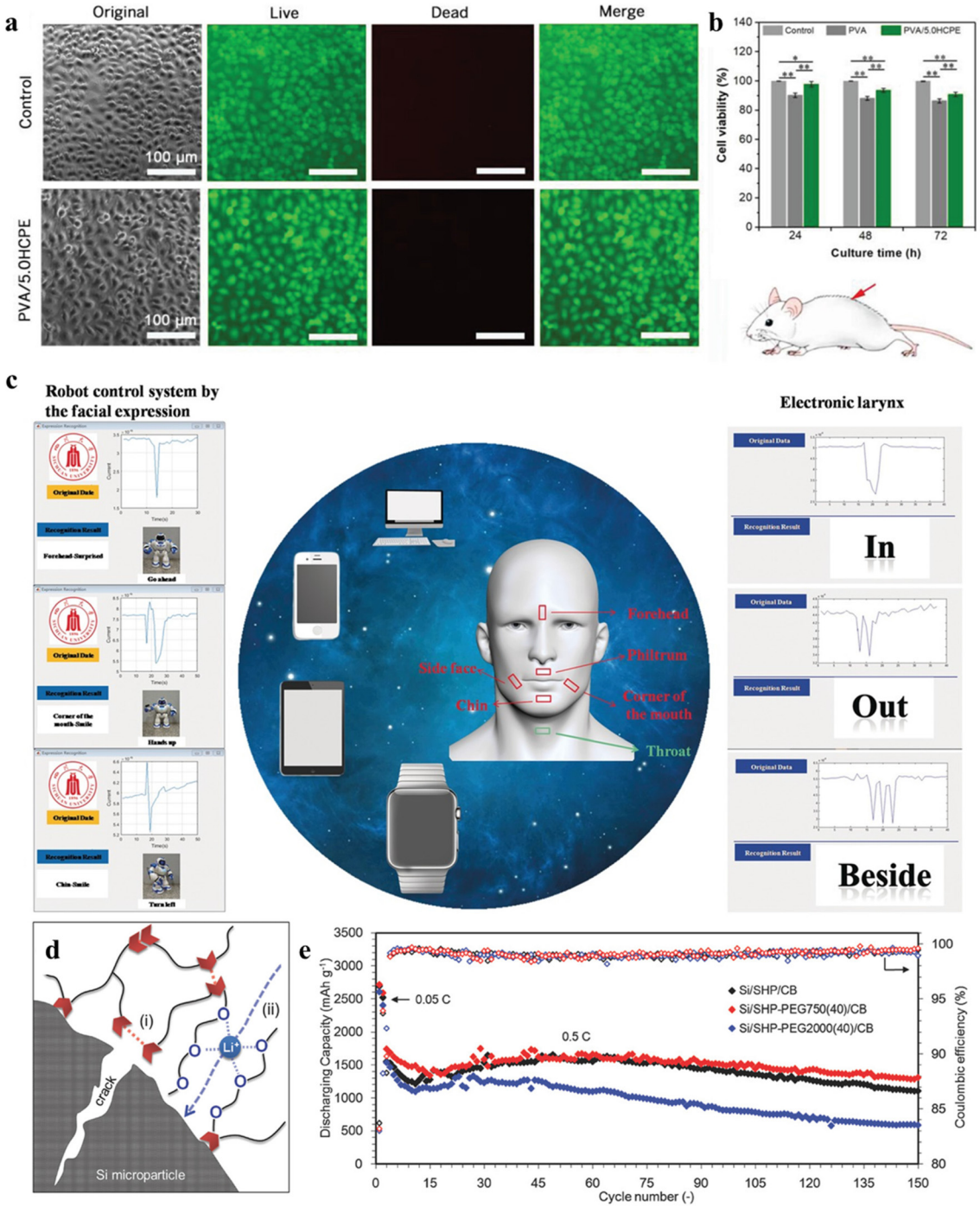

Fig. 12 (a) Fluorescence photographs from a live/dead assay depicting HUVECs cultured on PVA/HCPE for a duration of 72 hours. (b) Evaluation of cell toxicity in polymeric films after culturing HUVECs for 24, 48, and 72 hours. (a and b) Reproduced with permission.[67] © 2021 Wiley-VCH GmbH. (c) Human–machine interaction system showcasing facial expression (left) and speech (right) detection using strain sensors made from a supramolecular multiple hydrogen-bonded network elastomer and signal processing software. Reproduced with permission.[108] © 2017 Wiley-VCH Verlag GmbH & Co. KGaA, Weinheim. (d) A self-healing polymeric (SHP–PEG) binder, engineered with optimized viscoelasticity and stretchability through multiple hydrogen bonding interactions, designed to preserve the structural integrity of Si electrodes throughout charge–discharge cycling. (e) Cycling performance and coulombic efficiency of Si electrodes with different PEG binders. (d and e) Reproduced with permission.[109] © 2018 Wiley-VCH Verlag GmbH & Co. KGaA, Weinheim.

Bao *et al.*[109] reported another intriguing application of self-healing H-bonded cross-linked polymeric materials by incorporating poly(ethylene glycol) (PEG) as a binder in silicon electrodes (Fig. 12d). Through multiple H-bond interactions, the self-healing ability of PEG efficiently preserved the integrity of the interface between silicon nanoparticles and electrolytes by

optimizing the chemical structure. The resulting lithium-ion battery showed a good discharge capacity value of 2600 mAh g^{-1} and good cycling properties (Fig. 12e). After the H-bonded binder film was scraped and left to repair at ambient temperature, excellent self-healing was seen, as well. The approach shows promise for future high-capacity batteries experiencing significant volume changes or damage during cycling.

Adoption of exclusively hydrogen-bonded cross-linked networks on an industrial scale remains rare, despite strong research interest. The Cartiva® Synthetic Cartilage Implant, which was approved by the U.S. Food and Drug Administration (FDA) to treat osteoarthritis in the first metatarsophalangeal joint, is among the most prominent biomedical uses.[110] Physically cross-linked PVA hydrogels are used to create this implant, and repeated freeze–thaw cycles promote the development of hydrogen-bonded crystallite domains.[111] The implant has long-term *in vivo* stability, cartilage-like viscoelasticity, and adjustable mechanical qualities thanks to these reversible physical cross-links.

In the industrial sector, hot-melt adhesives represent one of the most widespread uses of multiple hydrogen-bonded polymer networks. Such adhesives are generally employed in electronics, filtration, and automotive and aerospace manufacturing. For example, Henkel's TECHNOMELT® PA line of polyamide-based hot-melt adhesives offers high strength, flexibility, and chemical and heat resistance, with strong inter-chain hydrogen bonds (https://www.henkel-adhesives.com/au/en/products/industrial-adhesives/hot-melt-adhesives.html). Arkema's Reverlink™, a self-healing elastomer with reversible intermolecular interactions, is another commercial example (https://www.arkema.com/global/en/media/newslist/news/global/innovation/2009/20090527-self-healing-elas/). This

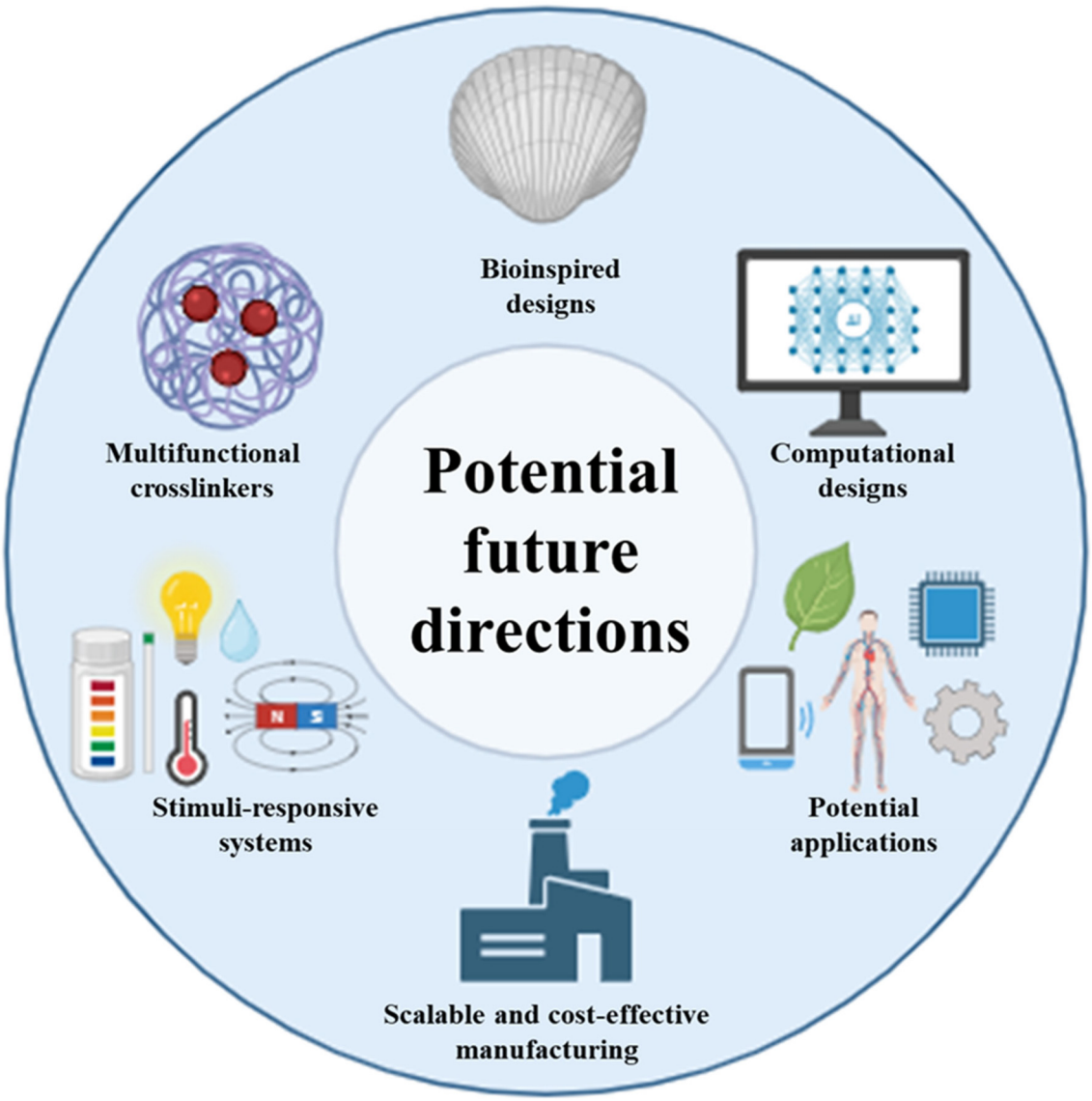

Fig. 13 Schematic illustration of potential future research directions for multiple hydrogen-bonded polymeric networks.

material features a three-dimensional network of small molecules and oligomers with multi-site hydrogen bonding interactions at both terminal and backbone sites.[112,113] The reversible nature of H-bonds allows the material to recover nearly all of its original strength after being cut or scratched under gentle pressure at room temperature without the need for healing agents or external stimuli.

7. Conclusions and outlook

Recently, hydrogen-bonded cross-linking has been widely utilized to tailor the mechanical properties of polymeric materials. The reversible nature of hydrogen-bonded cross-linking enables these materials to exhibit unique mechanical behaviour and self-healing capability. Relatively, different hydrogen bonds are easy to create *via* a range of approaches such as adding particle-based cross-linkers. This approach enables precise tuning of mechanical performance, making these materials suitable for demanding applications.

Hydrogen-bonded networks have inherent drawbacks despite their benefits. One major issue is that hydrogen bonds can easily be disrupted by moisture, which can gradually weaken their mechanical strength, especially under humid conditions.[114] While it might seem like a downside at first, the sensitivity to moisture has been utilized to develop water-responsive materials. These materials can trigger self-healing and adapt their mechanical properties in a controlled way.[115,116] Moreover, this type of polymeric material often displays hysteresis under cyclical tensile loading because the reformation of disrupted hydrogen bonds takes a certain amount of time.[117] Nonetheless, this hysteresis can be beneficial, as it aids in dissipating fracture energy during deformation, thereby contributing to improved fracture toughness. These aspects must be carefully considered and, where possible, used in the design of next-generation high-performance polymeric materials.

Looking ahead, the field of multi-hydrogen-bonded polymer networks has a great deal of scope for revolutionary advances along several novel research directions, as schematically illustrated in Fig. 13. For example, by taking inspiration from nature, such as the hierarchical designs of nacre that incorporate multiple hydrogen bonds, multi-scale energy dissipation pathways that achieve a remarkable balance between toughness and strength can be designed. Another fascinating direction is the development of stimuli-responsive systems, which adapt to various external stimuli, not just humidity, to offer accurate, on-demand control for smart applications. Multifunctional particle-based cross-linkers can increase their potential uses by enhancing mechanical strength, self-healing, and other characteristics like conductivity, biodegradability, or bioactivity. Computational design technologies such as machine learning, molecular dynamics, and density functional theory can speed up these developments, as well. Beyond their current and emerging uses, these high-performance polymeric materials hold great promise for entirely new and revolutionary applications. To bridge the gap between laboratory prototypes and large-scale commercial production, future efforts should concentrate on scalable and cost-effective fabrication techniques from an industrial and manufacturing perspective.

Author contributions

Pouya Rajaee: writing – review & editing, writing – original draft, visualization, methodology, formal analysis, data curation, conceptualization. Ishara Wijesinghe: writing – review & editing. Zhiyong Li: writing – review & editing. Cheng Yan: writing – review & editing, validation, supervision, formal analysis.

Conflicts of interest

The authors declare that they have no known competing financial interests or personal relationships that could have appeared to influence the work reported in this paper.

Data availability

No primary research results, software or code have been included and no new data were generated or analysed as part of this review.

Acknowledgements

Pouya Rajaee is grateful for the QUT Postgraduate Research Award (QUTPRA), and PhD scholarship from Queensland University of Technology, Brisbane, Australia.

References

1 V. R. Feig, H. Tran and Z. Bao, Biodegradable Polymeric Materials in Degradable Electronic Devices, *ACS Cent. Sci.*, 2018, **4**, 337–348.
2 L. Mandal, B. Verma, P. K. Patel, *et al.*, Review on polymer nanocomposite for ballistic & aerospace applications, *Mater. Today: Proc.*, 2020, 3161–3166.
3 J. M. Chalovich and E. Eisenberg, Synthetic biodegradable functional polymers for tissue engineering: a brief review, *Sci. China: Chem.*, 2014, **57**, 490–500.
4 A. Kl and J. Lei, Bio-inspired design of multiscale structures for function integration, *Nano Today*, 2011, **6**, 155–175.
5 G. Zhou, L. Li, D. W. Wang, X. Y. Shan, S. Pei, F. Li and H. M. Cheng, A flexible sulfur-graphene-polypropylene separator integrated electrode for advanced Li-S batteries, *Adv. Mater.*, 2015, **27**, 641–647.
6 S. Wan, J. Peng, L. Jiang and Q. Cheng, Bioinspired Graphene-Based Nanocomposites and Their Application

in Flexible Energy Devices, *Adv. Mater.*, 2016, **28**, 7862–7898.

7 J. Ge, L. Sun, F. R. Zhang, Y. Zhang, L. A. Shi, H. Y. Zhao, H. W. Zhu, H. L. Jiang and S. H. Yu, A Stretchable Electronic Fabric Artificial Skin with Pressure-, Lateral Strain-, and Flexion-Sensitive Properties, *Adv. Mater.*, 2016, **28**, 722–728.

8 H. Bin Yao, J. Ge, C. F. Wang, X. Wang, W. Hu, Z. J. Zheng, Y. Ni and S. H. Yu, A flexible and highly pressure-sensitive graphene-polyurethane sponge based on fractured microstructure design, *Adv. Mater.*, 2013, **25**, 6692–6698.

9 L. L. Li, G. Bin Qi, F. Yu, S. J. Liu and H. Wang, An adaptive biointerface from self-assembled functional peptides for tissue engineering, *Adv. Mater.*, 2015, **27**, 3181–3188.

10 R. O. Ritchie, The conflicts between strength and toughness, *Nat. Mater.*, 2011, **10**, 817–822.

11 H. Wan, B. Wu, L. Hou and P. Wu, Amphibious Polymer Materials with High Strength and Superb Toughness in Various Aquatic and Atmospheric Environments, *Adv. Mater.*, 2024, **36**, 2307290.

12 M. Irigoyen, A. Fernandez, A. Ruiz, F. Ruiperez and J. M. Matxain, Diselenide bonds as an alternative to outperform the efficiency of disulfides in self-healing materials, *J. Org. Chem.*, 2019, **84**, 4200–4210.

13 S. Cho, S. Y. Hwang, D. X. Oh and J. Park, Recent progress in self-healing polymers and hydrogels based on reversible dynamic B–O bonds: boronic/boronate esters, borax, and benzoxaborole, *J. Mater. Chem. A*, 2021, **9**, 14630–14655.

14 G. P. Carden, M. L. Martins, G. Toleutay, S. Ge, B. Li, S. Zhao and A. P. Sokolov, Critical role of free amine groups in the imine bonds exchange in dynamic covalent networks, *Macromolecules*, 2024, **57**, 8621–8631.

15 J. Canadell, H. Goossens and B. Klumperman, Self-healing materials based on disulfide links, *Macromolecules*, 2011, **44**, 2536–2541.

16 Y. V. Pereverzev, O. V. Prezhdo and L. R. Dalton, Structural origin of the enhanced electro-optic response of dendrimeric systems, *Chem. Phys. Lett.*, 2003, **373**, 207–212.

17 D. Mozhdehi, S. Ayala, O. R. Cromwell and Z. Guan, Self-healing multiphase polymers via dynamic metal-ligand interactions, *J. Am. Chem. Soc.*, 2014, **136**, 16128–16131.

18 Q. Zhang, S. Niu, L. Wang, J. Lopez, S. Chen, Y. Cai, R. Du, Y. Liu, J. C. Lai, L. Liu, C. H. Li, X. Yan, C. Liu, J. B. H. Tok, X. Jia and Z. Bao, An Elastic Autonomous Self-Healing Capacitive Sensor Based on a Dynamic Dual Crosslinked Chemical System, *Adv. Mater.*, 2018, **30**, 1801435.

19 A. Sanchez-Sanchez, A. Arbe, J. Colmenero and J. A. Pomposo, Metallo-folded single-chain nanoparticles with catalytic selectivity, *ACS Macro Lett.*, 2014, **3**, 439–443.

20 Z. Li, Y. Shan, X. Wang, H. Li, K. Yang and Y. Cui, Self-healing flexible sensor based on metal-ligand coordination, *Chem. Eng. J.*, 2020, **394**, 124932.

21 H. Xie, X. Liu, D. Sheng, H. Wu, Y. Zhou, X. Tian, Y. Sun, B. Shi and Y. Yang, Novel titin-inspired high-performance polyurethanes with self-healing and recyclable capacities based on dual dynamic network, *Polymer*, 2021, **230**, 124096.

22 Y. Yao, B. Liu, Z. Xu, J. Yang and W. Liu, An unparalleled H-bonding and ion-bonding crosslinked waterborne polyurethane with super toughness and unprecedented fracture energy, *Mater. Horiz.*, 2021, **8**, 2742–2749.

23 J. Yan, M. Li, Z. Wang, C. Chen, C. Ma and G. Yang, Highly tough, multi-stimuli-responsive, and fast self-healing supramolecular networks toward strain sensor application, *Chem. Eng. J.*, 2020, **389**, 123468.

24 B. Liu, Z. Tang, Z. Wang, L. Zhang and B. Guo, Integrating transient and sacrificial bonds into biobased elastomers toward mechanical property enhancement and macroscopically responsive property, *Polymer*, 2019, **184**, 121914.

25 M. Ahmadi and S. Seiffert, Coordination Geometry Preference Regulates the Structure and Dynamics of Metallo-Supramolecular Polymer Networks, *Macromolecules*, 2021, **54**, 1388–1400.

26 C. H. Li, C. Wang, C. Keplinger, J. L. Zuo, L. Jin, Y. Sun, P. Zheng, Y. Cao, F. Lissel, C. Linder, X. Z. You and Z. Bao, A highly stretchable autonomous self-healing elastomer, *Nat. Chem.*, 2016, **8**, 618–624.

27 J. C. Lai, X. Y. Jia, D. P. Wang, Y. B. Deng, P. Zheng, C. H. Li, J. L. Zuo and Z. Bao, Thermodynamically stable whilst kinetically labile coordination bonds lead to strong and tough self-healing polymers, *Nat. Commun.*, 2019, **10**, 1164.

28 Y. Sheng, M. Wang, K. Zhang, Z. Wu, Y. Chen and X. Lu, An "inner soft external hard", scratch-resistant, self-healing waterborne poly(urethane-urea) coating based on gradient metal coordination structure, *Chem. Eng. J.*, 2021, **426**, 131883.

29 Y. Song, Y. Liu, T. Qi and G. L. Li, Towards Dynamic but Supertough Healable Polymers through Biomimetic Hierarchical Hydrogen-Bonding Interactions, *Angew. Chem., Int. Ed.*, 2018, **57**, 13838–13842.

30 J.-M. Lehn, Supramolecular Chemistry-Scope and Perspectives Molecules, Supermolecules, and Molecular Devices (Nobel Lecture), *Angew. Chem., Int. Ed. Engl.*, 1988, **27**, 89–112.

31 P. Song, J. Dai, G. Chen, Y. Yu, Z. Fang, W. Lei, S. Fu, H. Wang and Z. G. Chen, Bioinspired Design of Strong, Tough, and Thermally Stable Polymeric Materials via Nanoconfinement, *ACS Nano*, 2018, **12**, 9266–9278.

32 J. Cao, Z. Zhou, Q. Song, K. Chen, G. Su, T. Zhou, Z. Zheng, C. Lu and X. Zhang, Ultrarobust Ti3C2TxMXene-Based Soft Actuators via Bamboo-Inspired Mesoscale Assembly of Hybrid Nanostructures, *ACS Nano*, 2020, **14**, 7055–7065.

33 S. Sun, Y. Xue, X. Xu, L. Ding, Z. Jiang, L. Meng, P. Song and Y. Bai, Highly Stretchable, Ultratough, and Strong Polyesters with Improved Postcrystallization Optical Property Enabled by Dynamic Multiple Hydrogen Bonds, *Macromolecules*, 2021, **54**, 1254–1266.

34 J. A. Fernández, Exploring hydrogen bond in biological molecules, *J. Indian Inst. Sci.*, 2020, **100**, 135–154.
35 R. E. Hubbard and M. K. Haider, Hydrogen bonds in proteins: role and strength, in *Encycl. Life Sci*, 2010.
36 P. Kolandaivel and V. Nirmala, Study of proper and improper hydrogen bonding using Bader's atoms in molecules (AIM) theory and NBO analysis, *J. Mol. Struct.*, 2004, **694**, 33–38.
37 X. Zhao, X. Z. Wang, X. K. Jiang, Y. Q. Chen, Z. T. Li and G. J. Chen, Hydrazide-Based Quadruply Hydrogen-Bonded Heterodimers. Structure, Assembling Selectivity, and Supramolecular Substitution, *J. Am. Chem. Soc.*, 2003, **125**, 15128–15139.
38 S. C. C. Van Der Lubbe, F. Zaccaria, X. Sun and C. F. Guerra, Secondary Electrostatic Interaction Model Revised: Prediction Comes Mainly from Measuring Charge Accumulation in Hydrogen-Bonded Monomers, *J. Am. Chem. Soc.*, 2019, **141**, 4878–4885.
39 F. H. Beijer, R. P. Sijbesma, H. Kooijman, A. L. Spek and E. W. Meijer, Strong dimerization of ureidopyrimidones via quadruple hydrogen bonding, *J. Am. Chem. Soc.*, 1998, **120**, 6761–6769.
40 F. H. Beijer, H. Kooijman, A. L. Spek, R. P. Sijbesma and E. W. Meijer, Self-complementarity achieved through quadruple hydrogen bonding, *Angew. Chem., Int. Ed.*, 1998, **37**, 75–78.
41 A. T. Ten Cate, H. Kooijman, A. L. Spek, R. P. Sijbesma and E. W. Meijer, Conformational Control in the Cyclization of Hydrogen-Bonded Supramolecular Polymers, *J. Am. Chem. Soc.*, 2004, **126**, 3801–3808.
42 G. B. W. L. Ligthart, H. Ohkawa, R. P. Sijbesma and E. W. Meijer, Complementary quadruple hydrogen bonding in supramolecular copolymers, *J. Am. Chem. Soc.*, 2005, **127**, 810–811.
43 B. J. B. Folmer, R. P. Sijbesma, H. Kooijman, A. L. Spek and E. W. Meijer, Cooperative dynamics in duplexes of stacked hydrogen-bonded moieties, *J. Am. Chem. Soc.*, 1999, **121**, 9001–9007.
44 P. S. Corbin, S. C. Zimmerman, P. A. Thiessen, N. A. Hawryluk and T. J. Murray, Complexation-induced unfolding of heterocyclic ureas. Simple foldamers equilibrate with multiply hydrogen-bonded sheetlike structures, *J. Am. Chem. Soc.*, 2001, **123**, 10475–10488.
45 E. S. Brielle and I. T. Arkin, Quantitative Analysis of Multiplex H-Bonds, *J. Am. Chem. Soc.*, 2020, **142**, 14150–14157.
46 Y. Yang, X. Ding and M. W. Urban, Chemical and physical aspects of self-healing materials, *Prog. Polym. Sci.*, 2015, 34–59.
47 N. Roy, B. Bruchmann and J. M. Lehn, DYNAMERS: Dynamic polymers as self-healing materials, *Chem. Soc. Rev.*, 2015, **44**, 3786–3807.
48 R. Hou, G. Li, Y. Zhang, M. Li, G. Zhou and X. Chai, Self-Healing Polymers Materials Based on Dynamic Supramolecular Motifs, *Prog. Chem.*, 2019, **31**, 690–698.
49 T. Kawakami and T. Kato, Use of intermolecular hydrogen bonding between imidazolyl moieties and carboxylic acids for the supramolecular self-association of liquid-crystalline side-chain polymers and networks, *Macromolecules*, 1998, **31**, 4475–4479.
50 L. Liu, M. Zhu, Z. Ma, X. Xu, J. Dai, Y. Yu, S. Mohsen Seraji, H. Wang and P. Song, Small multiamine molecule enabled fire-retardant polymeric materials with enhanced strength, toughness, and self-healing properties, *Chem. Eng. J.*, 2022, **440**, 135645.
51 X. Zhang, W. Liu, D. Yang and X. Qiu, Biomimetic Supertough and Strong Biodegradable Polymeric Materials with Improved Thermal Properties and Excellent UV-Blocking Performance, *Adv. Funct. Mater.*, 2019, **29**, 1806912.
52 D. K. Buslov, N. I. Sushko and O. N. Tretinnikov, IR investigation of hydrogen bonds in weakly hydrated films of poly(vinyl alcohol), *Polym. Sci., Ser. A*, 2011, **53**, 1121–1127.
53 D. S. Bag, S. Tiwari and K. M. Meenu, Chiral copolymers of (R)-N-(1-phenyl-ethyl) methacrylamide (R-NPEMAM) and 2-hydroxy ethyl methacrylate (HEMA): investigation of physico-chemical behavior, thermal properties and degradation kinetics, *J. Polym. Mater.*, 2023, **40**, 105–123.
54 T. Zhou, F. Chen, C. Tang, H. Bai, Q. Zhang, H. Deng and Q. Fu, The preparation of high performance and conductive poly (vinyl alcohol)/graphene nanocomposite via reducing graphite oxide with sodium hydrosulfite, *Compos. Sci. Technol.*, 2011, **71**, 1266–1270.
55 C. J. Seliskar and R. E. Hoffmann, On the infrared spectrum of malonaldehyde, a tunneling hydrogen-bonded molecule, *J. Mol. Spectrosc.*, 1982, **96**, 146–155.
56 P. Song, Z. Xu, Y. Lu and Q. Guo, Bio-Inspired Hydrogen-Bond Cross-Link Strategy toward Strong and Tough Polymeric Materials, *Macromolecules*, 2015, **48**, 3957–3964.
57 M. Qian, Y. Sun, X. Xu, L. Liu, P. Song, Y. Yu, H. Wang and J. Qian, 2D-alumina platelets enhance mechanical and abrasion properties of PA612 via interfacial hydrogen-bond interactions, *Chem. Eng. J.*, 2017, **308**, 760–771.
58 S. H. Hwang, D. Kang, R. S. Ruoff, H. S. Shin and Y. Bin Park, Poly(vinyl alcohol) reinforced and toughened with poly(dopamine)-treated graphene oxide, and its use for humidity sensing, *ACS Nano*, 2014, **8**, 6739–6747.
59 Q. Wu, Y. Shangguan, M. Du, J. Zhou, Y. Song and Q. Zheng, Steady and dynamic rheological behaviors of sodium carboxymethyl cellulose entangled semi-dilute solution with opposite charged surfactant dodecyl-trimethylammonium bromide, *J. Colloid Interface Sci.*, 2009, **339**, 236–242.
60 D. Zhao, Z. Zhang, J. Zhao, K. Liu, Y. Liu, G. Li, X. Zhang, R. Bai, X. Yang and X. Yan, A Mortise–and–Tenon Joint Inspired Mechanically Interlocked Network, *Angew. Chem.*, 2021, **133**, 16360–16365.
61 G. M. Scheutz, J. J. Lessard, M. B. Sims and B. S. Sumerlin, Adaptable Crosslinks in Polymeric Materials: Resolving the Intersection of Thermoplastics and Thermosets, *J. Am. Chem. Soc.*, 2019, **141**, 16181–16196.

62 K. Yu, M. Wang, J. Wu, K. Qian, J. Sun and X. Lu, Modification of the interfacial interaction between carbon fiber and epoxy with carbon hybrid materials, *Nanomaterials*, 2016, **6**(5), 89.
63 E. H. Qua, P. R. Hornsby, H. S. S. Sharma, G. Lyons and R. D. Mccall, Preparation and characterization of Poly (vinyl alcohol) nanocomposites made from cellulose nanofibers, *J. Appl. Polym. Sci.*, 2009, **113**, 2238–2247.
64 L. Liu, X. Xu, M. Zhu, X. Cui, J. Feng, Z. F. Rad, H. Wang and P. Song, Bioinspired Strong, Tough, and Biodegradable Poly(Vinyl Alcohol) and its Applications as Substrates for Humidity Sensors, *Adv. Mater. Technol.*, 2023, **8**, 2201414.
65 P. Song, Z. Xu and Q. Guo, Bioinspired strategy to reinforce PVA with improved toughness and thermal properties via hydrogen-bond self-assembly, *ACS Macro Lett.*, 2013, **2**, 1100–1104.
66 L. Li, X. Xu, L. Liu, P. Song, Q. Cao, Z. Xu, Z. Fang and H. Wang, Water governs the mechanical properties of poly (vinyl alcohol), *Polymer*, 2021, **213**, 123330.
67 L. Liu, M. Zhu, X. Xu, X. Li, Z. Ma, Z. Jiang, A. Pich, H. Wang and P. Song, Dynamic Nanoconfinement Enabled Highly Stretchable and Supratough Polymeric Materials with Desirable Healability and Biocompatibility, *Adv. Mater.*, 2021, **33**, 2105829.
68 R. Panigrahi, S. Chakraborty, J. Ye, G. S. Lim, F. C. H. Lim, J. K. H. Yam, L. Y. Wu, S. Chng, M. Prawirasatya, A. M. van Herk and P. Thoniyot, Elucidating the Role of Interfacial Hydrogen Bonds on Glass Transition Temperature Change in a Poly(Vinyl Alcohol)/SiO_2 Polymer-Nanocomposite by Noncovalent Interaction Characterization and Atomistic Molecular Dynamics Simulations, *Macromol. Rapid Commun.*, 2020, **41**, 2000240.
69 W. Xie, Q. Bao, Y. Liu, H. Wen and Q. Wang, Hydrogen Bond Association to Prepare Flame Retardant Polyvinyl Alcohol Film with High Performance, *ACS Appl. Mater. Interfaces*, 2021, **13**, 5508–5517.
70 X. Xu, L. Li, S. M. Seraji, L. Liu, Z. Jiang, Z. Xu, X. Li, S. Zhao, H. Wang and P. Song, Bioinspired, Strong, and Tough Nanostructured Poly(vinyl alcohol)/Inositol Composites: How Hydrogen-Bond Cross-Linking Works?, *Macromolecules*, 2021, **54**, 9510–9521.
71 P. J. Taenzler, K. Sadeghian and C. Ochsenfeld, Theoretical investigations of the hydrogen bond in a tetra-amido/diamino quaternized macrocycle, *Mol. Phys.*, 2019, **117**, 1276–1286.
72 G. Gunnarsson, H. Wennerström, W. Egan and S. Forsén, Proton and deuterium NMR of hydrogen bonds: Relationship between isotope effects and the hydrogen bond potential, *Chem. Phys. Lett.*, 1976, **38**, 96–99.
73 R. Konrat, M. Tollinger, G. Kontaxis and B. Kräutler, NMR Techniques to Study Hydrogen Bonding in Aqueous Solution, in *Hydrog. Bond Res*, 1999, pp. 17–38.
74 M. M. Coleman, J. F. Graf and P. C. Painter, Specific interactions and the miscibility of polymer blends, in *Specif. Interact. Miscibility Polym. Blends*, 2017, pp. 1–516.
75 Z. Guo, Y. Qu, C. Tian, M. Su and H. M. Yin, Constructing stretchable, tough, and stiff fluoroelastomer via tannic acid self-assembly, *Colloids Surf., A*, 2023, **666**, 131320.
76 J. Chen, J. Jing, C. Wang, T. Chen, J. Xu, B. Yao and J. Fu, Ultra-strong, ultra-tough, and transparent polymer composite with excellent dynamic and biodegradable properties enabled by bicontinuous structure, *Polymer*, 2023, **283**, 126220.
77 T. Kashiwagi, F. Du, J. F. Douglas, K. I. Winey, R. H. Harris and J. R. Shields, Nanoparticle networks reduce the flammability of polymer nanocomposites, *Nat. Mater.*, 2005, **4**, 928–933.
78 P. Song, L. Xu, Z. Guo, Y. Zhang and Z. Fang, Flame-retardant-wrapped carbon nanotubes for simultaneously improving the flame retardancy and mechanical properties of polypropylene, *J. Mater. Chem.*, 2008, **18**, 5083–5091.
79 Y. Hu, C. L. Bao, Y. Q. Guo and L. Song, Poly(vinyl alcohol) nanocomposites based on graphene and graphite oxide: a comparative investigation of property and mechanism, *J. Mater. Chem.*, 2011, **21**, 13942–13950.
80 P. Rittigstein, R. D. Priestley, L. J. Broadbelt and J. M. Torkelson, Model polymer nanocomposites provide an understanding of confinement effects in real nanocomposites, *Nat. Mater.*, 2007, **6**, 278–282.
81 X. Qin, W. Xia, R. Sinko and S. Keten, Tuning Glass Transition in Polymer Nanocomposites with Functionalized Cellulose Nanocrystals through Nanoconfinement, *Nano Lett.*, 2015, **15**, 6738–6744.
82 Y. Guan, W. Li, Y. Zhang, Z. Shi, J. Tan, F. Wang and Y. Wang, Aramid nanofibers and poly (vinyl alcohol) nanocomposites for ideal combination of strength and toughness via hydrogen bonding interactions, *Compos. Sci. Technol.*, 2017, **144**, 193–201.
83 Y. Shi, C. Liu, L. Liu, L. Fu, B. Yu, Y. Lv, F. Yang and P. Song, Strengthening, toughing and thermally stable ultra-thin MXene nanosheets/polypropylene nanocomposites via nanoconfinement, *Chem. Eng. J.*, 2019, **378**, 122267.
84 L. Liu, M. Zhu, Y. Shi, X. Xu, Z. Ma, B. Yu, S. Fu, G. Huang, H. Wang and P. Song, Functionalizing MXene towards highly stretchable, ultratough, fatigue- and fire-resistant polymer nanocomposites, *Chem. Eng. J.*, 2021, **424**, 130338.
85 C. Liu, K. Xu, Y. Shi, J. Wang, S. Ma, Y. Feng, Y. Lv, F. Yang, M. Liu and P. Song, Fire-safe, mechanically strong and tough thermoplastic Polyurethane/MXene nanocomposites with exceptional smoke suppression, *Mater. Today Phys.*, 2022, **22**, 100607.
86 J. Li, P. Zhang, L. Chen, G. Li, H. Chen, C. Jia, Y. Wu, M. Chen, X. Zhao and P. Song, Strong, tough and healable elastomer nanocomposites enabled by a hydrogen-bonded supramolecular network, *Compos. Commun.*, 2020, **22**, 100530.
87 T. Zhang, Q. Yu, L. Fang, J. Wang, T. Wu and P. Song, All-Organic Multilayer Coatings for Advanced Poly(lactic acid)

Films with High Oxygen Barrier and Excellent Antifogging Properties, *ACS Appl. Polym. Mater.*, 2019, **1**, 3470–3476.

88 Y. Fang, J. Tong and S. Qiu, Bioinspired Strong and Tough Poly(ε-caprolactone)/Graphene Nanodot Composite Films via Weak Hydrogen Bonds: Implications for Thermal-Mechanical Properties, *ACS Appl. Nano Mater.*, 2023, **6**, 19088–19097.

89 J. Ding, H. Zhao, S. Shi, J. Su, Q. Chu, H. Wang, B. Fang, M. R. Miah, J. Wang and J. Zhu, High-Strength, High-Barrier Bio-Based Polyester Nanocomposite Films by Binary Multiscale Boron Nitride Nanosheets, *Adv. Funct. Mater.*, 2024, **34**, 2308631.

90 P. Song, Z. Xu, M. S. Dargusch, Z. G. Chen, H. Wang and Q. Guo, Granular Nanostructure: A Facile Biomimetic Strategy for the Design of Supertough Polymeric Materials with High Ductility and Strength, *Adv. Mater.*, 2017, **29**, 1704661.

91 S. Xiong, C. Zhang, R. Huang, K. Luo, X. Zhu and G. Tong, Strong yet tough, excellent thermal resistant and UV-Protective Polydopamine/Poly(vinyl alcohol) composites via hydrogen-bonding interaction, *Polymer*, 2021, **221**, 123603.

92 Y. Fang, S. Xiong, H. Huang, J. Zhu, J. Yu, Y. Wang and Z. Hu, Polydopamine nanotube for dual bio-inspired strong, tough, and flame retarding composites, *Composites, Part B*, 2020, **197**, 108184.

93 S. Xie and S. Dai, Visualizing small molecules via transmission electron microscopy, *Microstructures*, 2025, **5**, 2025057.

94 R. Chitas, D. R. Fonseca, P. Parreira and M. C. L. Martins, Targeted nanotherapeutics for the treatment of Helicobacter pylori infection, *J. Biomed. Sci.*, 2024, **31**, 78.

95 F. Cerrón-Mercado, B. K. Salva-Ruíz, D. Nolazco-Cama, C. Espinoza-Silva, J. Fernández-López, J. A. Pérez-Alvarez and M. Viuda-Martos, Development of chincho (Tagetes elliptica Sm.) essential oil organogel nanoparticles through ionic gelation and process optimization with Box–Behnken design, *Gels*, 2022, **8**, 815.

96 B. R. Maciel, K. Wang, M. Müller, C. Oelschlaeger and N. Willenbacher, Targeted micro-phase separation–a generic design concept to control the elasticity of extrudable hydrogels, *Mater. Des.*, 2023, **227**, 111803.

97 T. Zhao, J. Wang, Y. Liu, X. Li, Y. Bai, B. Luo and S. Nie, Self-healing and toughness triboelectric materials enabled by dynamic nanoconfinement quenching, *Adv. Funct. Mater.*, 2024, **34**, 2410096.

98 Z. Xie, B. L. Hu, R. W. Li and Q. Zhang, Hydrogen bonding in self-healing elastomers, *ACS Omega*, 2021, **6**, 9319–9333.

99 O. Lebel, T. Maris, M.È. Perron, E. Demers and J. D. Wuest, The dark side of crystal engineering: creating glasses from small symmetric molecules that form multiple hydrogen bonds, *J. Am. Chem. Soc.*, 2006, **128**, 10372–10373.

100 C. B. St. Pourcain and A. C. Griffin, Thermoreversible supramolecular networks with polymeric properties, *Macromolecules*, 1995, **28**, 4116–4121.

101 Z. Zhang, J. Luo, S. Zhao, S. Ge, J. M. Carrillo, J. K. Keum, C. Do, S. Cheng, Y. Wang, A. P. Sokolov and P. F. Cao, Surpassing the stiffness-extensibility trade-off of elastomers via mastering the hydrogen-bonding clusters, *Matter*, 2022, **5**, 237–252.

102 S. V. Wanasinghe, O. J. Dodo and D. Konkolewicz, Dynamic bonds: adaptable timescales for responsive materials, *Angew. Chem.*, 2022, **134**, e202206938.

103 M. L. Martins, X. Zhao, Z. Demchuk, J. Luo, G. P. Carden, G. Toleutay and A. P. Sokolov, Viscoelasticity of polymers with dynamic covalent bonds: concepts and misconceptions, *Macromolecules*, 2023, **56**, 8688–8696.

104 X. Hu, M. Vatankhah-Varnoosfaderani, J. Zhou, Q. Li and S. S. Sheiko, Weak hydrogen bonding enables hard, strong, tough, and elastic hydrogels, *Adv. Mater.*, 2015, **27**, 6899–6905.

105 S. Thiele, C. J. Plummer, L. Piveteau and H. Frauenrath, Dynamics of hydrogen-bonded end groups in bulk polymers revealed by solid-state NMR spectroscopy relaxation dispersion experiments, *Commun. Chem.*, 2025, **8**, 217.

106 Y. W. Ge, J. W. Lu, Z. Y. Sun, Z. Q. Liu, J. Zhou, Q. F. Ke, Y. Q. Mao, Y. P. Guo and Z. A. Zhu, Ursolic acid loaded-mesoporous bioglass/chitosan porous scaffolds as drug delivery system for bone regeneration, *Nanomedicine*, 2019, **18**, 336–346.

107 X. Yu, Y. Wang, X. Liu, Y. Ge and S. Zhang, Ursolic acid loaded-mesoporous hydroxylapatite/chitosan therapeutic scaffolds regulate bone regeneration ability by promoting the m2-type polarization of macrophages, *Int. J. Nanomed.*, 2021, **16**, 5301–5315.

108 J. Cao, C. Lu, J. Zhuang, M. Liu, X. Zhang, Y. Yu and Q. Tao, Multiple Hydrogen Bonding Enables the Self-Healing of Sensors for Human–Machine Interactions, *Angew. Chem., Int. Ed.*, 2017, **56**, 8795–8800.

109 T. Munaoka, X. Yan, J. Lopez, J. W. F. To, J. Park, J. B. H. Tok, Y. Cui and Z. Bao, Ionically Conductive Self-Healing Binder for Low Cost Si Microparticles Anodes in Li-Ion Batteries, *Adv. Energy Mater.*, 2018, **8**, 1703138.

110 J. F. Baumhauer, D. Singh, M. Glazebrook, C. Blundell, G. De Vries, I. L. Le and on behalf of the CARTIVA Motion Study Group, Prospective, randomized, multi-centered clinical trial assessing safety and efficacy of a synthetic cartilage implant versus first metatarsophalangeal arthrodesis in advanced hallux rigidus, *Foot Ankle Int.*, 2016, **37**, 457–469.

111 D. Murugan, H. Arumugam, S. Arumugam, M. Mani and S. Kannan, Superparamagnetic freeze-thawed PVA hydrogel for applications in tissue engineering, drug delivery and bioimaging, *Colloids Surf., A*, 2024, **690**, 133790.

112 G. C. Stevens, Living dielectrics, *IEEE Electr. Insul. Mag.*, 2023, **39**, 7–33.

113 L. Pernigoni and A. M. Grande, Towards safer space suits with self-healing materials, in *16th Eur. Conf. Spacecr. Struct. Mater. Environ. Test. (ECSSMET 2021)*, 2021, pp. 1–7.

114 Z. C. Jiang, Y. Y. Xiao, Y. Kang, B. J. Li and S. Zhang, Semi–IPNs with moisture–triggered shape memory and self–healing properties, *Macromol. Rapid Commun.*, 2017, **38**, 1700149.

115 M. Liu, P. Liu, G. Lu, Z. Xu and X. Yao, Multiphase–assembly of siloxane oligomers with improved mechanical strength and water–enhanced healing, *Angew. Chem.*, 2018, **130**, 11412–11416.

116 K. Wei, X. Yu, X. Zhang, J. Cao, L. Bai, W. Wang and L. Yang, Self-healing, tough hydrogels with long-lasting moisture and extreme temperature tolerance and application for flexible sensors, *Chem. Eng. Sci.*, 2025, 122312.

117 M. C. Luo, J. Zeng, X. Fu, G. Huang and J. Wu, Toughening diene elastomers by strong hydrogen bond interactions, *Polymer*, 2016, **106**, 21–28.